RICE UNIVERSITY

Imaging in Cluttered Acoustic Waveguides

by

Leila Issa

A Thesis Submitted
in Partial Fulfillment of the
Requirements for the Degree

Master of Arts

Approved, Thesis Committee:

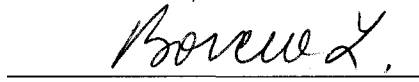

Liliana Borcea
Professor of Computational and Applied Mathematics

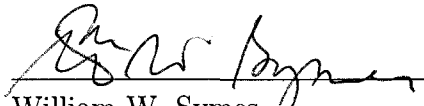

William W. Symes
Noah Harding Professor of Computational and Applied Mathematics

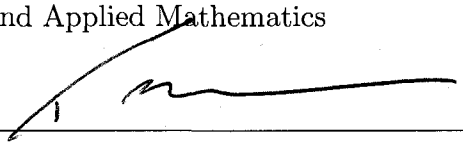

Tim Warburton
Assistant Professor of Computational and Applied Mathematics

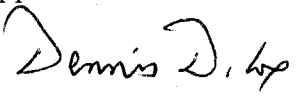

Dennis D. Cox
Professor of Statistics

Houston, Texas

October, 2007

Abstract

Imaging in Cluttered Acoustic Waveguides

by

Leila Issa

We consider an inverse problem for the acoustic scalar wave equation in a cluttered waveguide. The problem is to find the location of sources or scatterers, given measurements of the pressure at a remote array of transducers. The sound speed in the waveguide fluctuates rapidly due to the presence of small inhomogeneities. These fluctuations, not known in detail, are viewed as clutter and modeled as a random process. We consider the regime of weak fluctuations, $O(\epsilon)$, whose effect on the wavefield accumulates after long propagation distances, $O(1/\epsilon^2)$. This recorded field is backpropagated using the homogeneous Green's function to search points where an image is formed. The multiple scattering due to clutter may lead to significant loss of coherence in the data, which in turn can cause instability and loss of resolution in the images. Parameters such as frequency band, depth of the waveguide, number of modes and aperture play a major role in the resolution and stability of the resulting images.

Acknowledgements

I would like to express my gratitude to my advisor Dr. Liliana Borcea for all of her guidance. I would also like to thank the members of my committee Dr. William Symes, Dr. Tim Warburton and Dr. Dennis Cox. I thank Fernando Gonzalez Del Cueto for his help and support and my friends Mili Shah, Mona Sheikh, Joanna Papakonstantinou, Marco Enriquez, Rami Nammour and Ryan Nong for their support. I thank my parents Nahawand and Najib for their constant love and support, and my brothers Naji and Hadi for the comic relief.

Contents

List of Figures

Chapter 1

Introduction

1.1 Problem Definition and Motivation

This thesis considers the problem of imaging sources or scatterers in a waveguide occupying a spatial domain

$$\{\mathbf{x} = (x, y, z) \in \mathbb{R}^3,\, x \in [0, d]\}.$$

By imaging sources, we mean the estimation of their spatial support. By imaging scatterers, we mean finding the loci of jump discontinuities in the wave speed $c(\mathbf{x})$, where wave scattering occurs.

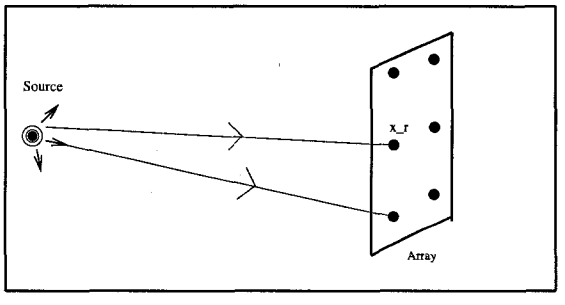

Figure 1.1: Source. The unknown source sends a signal that propagates in the waveguide. The time traces are recorded at antenna locations $x_r \in \mathcal{A}$.

The sources we wish to image may be small or distributed in some domain $\mathcal{D}$. These sources emit signals that propagate through the waveguide. To image them, we record the data that are time traces measured over some time window $[t_0, t_f]$, at a remote array of receivers $\mathcal{A}$, see Figure 1.1.

The data acquisition for imaging scatterers is done as follows: sources located at $x_s \in \mathcal{A}$ emit pulses that propagate through the waveguide and scatter at the reflectors supported in $\mathcal{D}$. At the array, we record the time traces of the echoes at receiver locations x_r, see Figure 1.2.

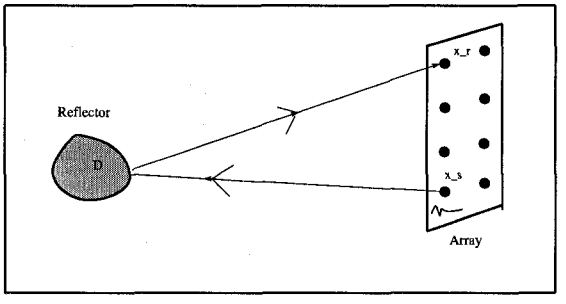

Figure 1.2: Reflector. Sources $x_s \in \mathcal{A}$ probe the waveguide; a wave propagates and is reflected from $\mathcal{D}$; the echoes are recorded at receivers $x_r \in \mathcal{A}$.

The imaging problem has a broad range of applications, specially in the domain of underwater acoustics. Examples are mapping of the sea floor, mine hunting, long range detection of submarines, and search for natural resources. Other applications may include imaging in corridors or tunnels.

In this thesis, we look at the problem in the context of underwater acoustics and we formulate it mathematically as an inverse scattering problem for the acoustic wave equation, in constant density media.

Imaging in waveguides with known and smooth wave speed is relatively well understood [8, 18, 22]. If the speed is not known but smooth, it is feasible to estimate it from the data using some velocity estimation techniques [23, 27]. In reality however, the wave speed may have rapid fluctuations due to ocean traffic, fish, or internal

waves [10, 22]. Such fluctuations cannot be estimated from the data, so we view them as clutter and model them with random processes. Clutter complicates the imaging process, because of the multiple scattering of the waves, which leads to traces that have coda, or delay spread. It is important to note here that the coda can not be viewed as uncorrelated instrument-like noise because it has some structure (correlation) encoded in it.

We approach the imaging problem from the point of view of separation of scales. More precisely, we view the index of refraction, defined by $n(\mathbf{x}) = \frac{c_0}{c(\mathbf{x})}$, where c_0 is some reference velocity, as follows

$$n^2(\mathbf{x}) = \overline{n}^2(\mathbf{x})(1 + \epsilon\mu(\mathbf{x})).$$

Here $\overline{n}(\mathbf{x})$ is smooth, and we suppose for simplicity that it is known. The fluctuations are modeled with a mean zero, normalized, random process μ. We use a small parameter ϵ to control the magnitude of the fluctuations.

The main goal of this thesis is to quantify the effect of the random fluctuations μ on imaging, and to develop statistically stable imaging techniques. By stable, we mean images that do not depend on the particular realization of the random process μ.

1.2 Previous Work

Before we give an overview of the content of this thesis, we go through a brief review of some studies that have been conducted on the topic of imaging in waveguides, in the context of underwater acoustics.

1.2.1 Imaging Scatterers in Shallow Water

In a series of papers [18, 16, 17], Gilbert et al. consider the problem of localizing scatterers in shallow water from measurements of the acoustic pressure field at two horizontal lines placed above the scatterer.

The shallow ocean is modeled as a two-dimensional ($2D$) waveguide. The imaging problem is formulated mathematically as finding the scattering potential $V(x,y)$ in the index of refraction $n(x,z)$ where

$$n^2(x,z) = \overline{n}^2(x) + V(x,z).$$

The background index of refraction $\overline{n}(x)$ is known and smooth and the potential is compactly supported in a subset $\mathcal{D}$ of the waveguide. In [18], the potential is estimated using linearized output least squares.

Dediu and McLaughlin in [9] consider a similar problem for a different measurement setup, where the transmitted and backscattered pressure fields are recorded at two vertical lines at each end of the waveguide. The inversion is still based on linearization (Born approximation) but it uses the spectral decomposition of the far-field matrix (whose entries are given by the propagating mode amplitudes) to obtain an analytical expression for the scattering potential.

None of the above imaging approaches take into account the effect of instrument noise or clutter.

1.2.2 Matched-Field

Kuperman et al [22, 3, 2] use Matched-Field (MF) methods to locate a point source in the ocean. These methods form an image by matching the measured array data to a waveguide propagation model, tested at hypothetical source locations $\mathbf{x}^s$.

In [3], the conventional MF function is given by

$$I^{(MF)}(\mathbf{x}^s) = \left| \sum_{i=1}^{M} \hat{d}(\mathbf{x_i}; \omega, \mathbf{x_0}) w(\mathbf{x}^s; \omega, \mathbf{x_i}) \right|^2, \tag{1.1}$$

where

$$w(\mathbf{x}^s; \omega, \mathbf{x_i}) = \frac{\overline{\hat{G}(\mathbf{x}^s; \omega, \mathbf{x_i})}}{|\hat{G}(\mathbf{x}^s; \omega, \mathbf{x}_i)|},$$

and $\hat{G}$ is the Green's function for the Helmholtz equation in a waveguide with piecewise smooth velocity $c(x)$. The source location is $\mathbf{x}_0$ and the data vectors $\hat{d}$ are measured at antenna positions $\mathbf{x}_i$, $i = 1, 2 \ldots M$, in frequency domain.

By defining the vector $\mathbf{w}(\mathbf{x}^s)$ whose entries are

$$w(\mathbf{x^s}; \omega, \mathbf{x}_i),$$

and $\hat{\mathbf{d}}$ with entries

$$\hat{d}_i = \hat{d}(\mathbf{x_i}; \omega, \mathbf{x_0}), \quad i = 1, \ldots M,$$

the imaging function (1.1) can be rewritten as

$$I^{(MF)}(\mathbf{x}^s) = \mathbf{w}^*(\mathbf{x}^s) \left(\sum_{i=1}^{M} \hat{d}_i \hat{d}_i^* \right) \mathbf{w}(\mathbf{x}^s) \,,$$

where * denotes conjugate transpose of a vector.

The data vectors $\hat{\mathbf{d}}$ are modeled as random variables with mean zero and covariance

$$\mathbf{K} = \mathbb{E}[\hat{\mathbf{d}}\hat{\mathbf{d}}^*].$$

The randomness in the data is due to external noise sources such as instrument noise, discrete noise sources or distributed noise sources at the surface of the ocean. Note that this is different from clutter, because it does not correspond to fluctuations in the wavespeed. Moreover, the noise is assumed to be additive; therefore the covariance matrix $\mathbf{K}$ can be then written as

$$\mathbf{K} = \mathbf{K_N} + \mathbf{K_S} \,,$$

where $\mathbf{K_N}$ corresponds to the covariance in the data due to noise and $\mathbf{K_S}$ is the covariance of the data without noise.

In practice, the covariance $\mathbf{K}$ is not known and it must be estimated. The Fourier transform of the data in sliding time windows could be used for that purpose. For example, if d^l is the data in the time window χ_l and its Fourier transform over χ_l is

denoted by $\hat{d}^l$, then an estimate of the covariance matrix is

$$\tilde{\mathbf{K}} = \frac{1}{L}\sum_{l=1}^{L} \hat{\mathbf{d}}^l \hat{\mathbf{d}}^{l^*}.$$

Using an estimation $\tilde{\mathbf{K}}$ of the covariance, the imaging functional (1.1) becomes

$$\tilde{I}^{(MF)}(\mathbf{x}^s) = \mathbf{w}^*(\mathbf{x}^s)\tilde{\mathbf{K}}\mathbf{w}(\mathbf{x}^s)\,. \tag{1.2}$$

An important observation is that whenever $\mathbf{w}(\mathbf{x}^s)$ projects on an eigenvector of $\mathbf{K}_{\mathrm{N}}$ corresponding to a large eigenvalue, the response of (1.2) will potentially mask the component of the true signal, introducing spurious sidelobes.

To minimize the sidelobe effects, the use of Maximum Likelihood Method (MLM) is proposed [3]. The MLM imaging functional is given by

$$I^{(MLM)}(\mathbf{x}^s) = \mathbf{w}_{\mathrm{ML}}(\mathbf{x}^s)^*\ \tilde{\mathbf{K}}\ \mathbf{w}_{\mathrm{ML}}(\mathbf{x}^s) \tag{1.3}$$

where $\mathbf{w}_{\mathrm{ML}}(\mathbf{x}^s)$ is the solution of the optimization problem

$$\begin{aligned} &\min\ \mathbf{w}_{\mathrm{ML}}^*(\mathbf{x}^s)\ \tilde{\mathbf{K}}\ \mathbf{w}_{\mathrm{ML}}(\mathbf{x}^s) \\ &\text{subject to } \left(\mathbf{w}_{\mathrm{ML}}(\mathbf{x}^s) - \mathbf{w}(\mathbf{x}^s)\right)^*\mathbf{w}(\mathbf{x}^s) = 0\,. \end{aligned}$$

It can be shown that, under certain signal-to-noise assumptions [3], (1.3) preserves the maximum of (1.3) while suppressing sidelobes effectively, thus improving resolution.

However, we must point out that the methods described above do not consider random fluctuations in the wavespeed, which cannot be simply added to the signal.

1.3 Outline

This thesis is organized as follows. Chapter 2, entirely based on the analysis done in [13], provides the necessary background for understanding long range wave propagation in the cluttered waveguide. The propagation is described by the acoustic

wave equation with an index of refraction that has fluctuations modeled as a random process. The Green's function in the cluttered waveguide is a superposition of coupled propagating and evanescent modes, whose amplitudes are unknown random functions. Using the diffusion limit, the mode amplitudes are shown to converge weakly as $\epsilon \to 0$ to a Markov process, whose first and second moments are computed. The first moment allows us to quantify the effect of the fluctuations on the expected pressure field. These fluctuations lead to loss of coherence by damping the mode amplitudes. They also introduce a phase shift for each mode.

In Chapter 3, we consider the migration imaging function, which consists of back-propagating the pressure field to a search domain where the image is formed, using the homogeneous Green's function. The results of Chapter 2 are used to obtain the expectation of the imaging function in a cluttered waveguide. We look at case where there is some coherence left, and we study numerically the stability and resolution properties of the migration imaging function, distinguishing between the broadband and narrowband cases. The numerical results show the stability of the images in the broadband case. These images have a slightly bigger spot in the range direction than the images in a homogeneous waveguide. The numerical results suggest that, in the narrowband case, having a large number of modes helps in achieving stability.

Finally, we give an outline of the directions for future research.

Chapter 2

Propagation in Random Waveguides

A prerequisite to study the effect of the random fluctuations on imaging is to understand how they affect long range wave propagation. The mathematical formulation of the problem is given by the acoustic scalar wave equation, with the sound speed having fluctuations modeled as random processes. We follow the model introduced by Kohler and Papanicolaou in [21], as well as Dozier and Tappert in [10], where the sound speed consists of a smooth part that depends on depth only. The random fluctuations vary with both range and depth. The fact that the smooth part depends on depth only is motivated by applications in the deep ocean, where the horizontal variations of the velocity, caused by geographical location, are much slower than the vertical ones, which are mainly due to temperature gradients, pressure and salinity [23, 22, 10]. As for the fluctuations, they are modeled as an effect of internal waves [10]. Other factors such as rough surfaces in the waveguide are neglected.

We consider first wave propagation in a smooth waveguide, without the fluctuations. In this simple case, the problem can be solved by separation of variables and the solution is a superposition of decoupled propagating and evanescent modes, with constant amplitudes. When we have fluctuations, the problem is not separable. The

modes are coupled by the fluctuations and they satisfy a system of stochastic differential equations. Kohler and Papanicolaou in [21], then Garnier and Papanicolaou in [15, 13] (see also Kirr and Weinstein [20]), provide the asymptotic analysis of these equations, in the limit $\epsilon \to 0$. In this chapter, we summarize some of their results that we need for our work.

Note that we consider here the wave-field due to a point source (Green's function). For distributed sources, the solution is a superposition of Green's functions. For scatterers, we can use the Born approximation to write the scattered wave-field in terms of the Green's function as well. For simplicity, we look at the two-dimensional ($2D$) problem. The analysis extends easily to three dimensions.

2.1 Formulation of the Wave Propagation Problem

2.1.1 The Acoustic Wave Equation for the Pressure Field

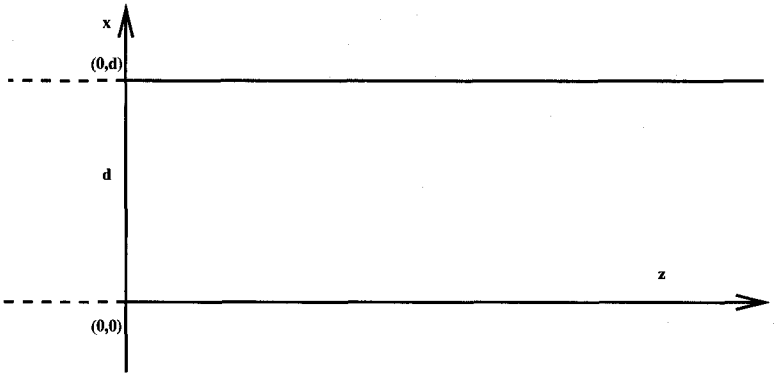

Figure 2.1: System of coordinates for a planar waveguide. $x \in [0, d]$ and $-\infty < z < \infty$.

The mathematical model for the propagation of acoustic waves is given by the

scalar wave equation

$$-\frac{1}{c^2(x,z)}\frac{\partial^2 p(x,z,t)}{\partial t^2} + \Delta p(x,z,t) = F(t,x,z), \quad t > 0,$$
$$p(x,z,t) = 0 \qquad \text{for} \quad t \leq 0, \tag{2.1}$$

where p is the pressure and $\Delta = \frac{\partial^2}{\partial x^2} + \frac{\partial^2}{\partial z^2}$ is the Laplace operator. We consider (2.1) in the strip

$$\Omega = \{(x,z) \in \mathbb{R}^2, \; s.t. \quad 0 \leq x \leq d\},$$

where d is the depth of the waveguide, and z is the range direction (direction of propagation), see Figure 2.1. The wave speed $c(x,z)$ is assumed to be time independent, because we suppose that the duration of the data collection experiment is much shorter than the time scale over which the medium changes.

Typical boundary conditions encountered in the literature are a pressure release (Dirichlet) condition

$$p(x,z,t) = 0 \quad \text{for} \quad x = 0 \quad \text{or} \quad d,$$

or a Neumann boundary condition to model rigid bottoms

$$\frac{\partial p}{\partial z}(0,z,t) = 0.$$

Alternatively, Robin boundary conditions could be imposed at $x = 0$, in order to model energy loss through radiation in the ocean's floor [24]. Another approach for modeling this radiation is considered in [21], where the depth of the waveguide is assumed infinite, but the wave-speed is constant for the sediments below the floor.

The analysis does not change in an essential way for any of the three types of conditions, Dirichlet, Neumann or Robin. The infinite depth case is more complicated, but it can be handled as shown in [21]. To fix ideas, we take Dirichlet boundary conditons on the top and at the bottom

$$p(0,z,t) = 0, \quad p(d,z,t) = 0.$$

The source term in (2.1) is given by

$$F(x,z,t) = \nabla \cdot \mathbf{h}(x,z,t),$$

where $\mathbf{h}$ is the external force density, assumed to be of the form

$$\mathbf{h}(x,z,t) = f(t)\delta(x-x_0)\delta(z-z_0)\mathbf{e}_z, \quad \mathbf{e}_z = \begin{bmatrix} 1 \\ 0 \end{bmatrix}. \tag{2.2}$$

This gives

$$F(x,z,t) = f(t)\delta(x-x_0)\delta'(z-z_0). \tag{2.3}$$

and it models a point source at (x_0, z_0) emitting a pulse $f(t)$ in the z direction. We take

$$f(t) = e^{-i\omega_0 t} f_B(t),$$

where f_B is the base band pulse, ω_0 is the central frequency and B is the bandwidth, defined as the support of the Fourier transform of f,

$$\hat{f}(\omega) = \int_{-\infty}^{\infty} e^{i(\omega-\omega_0)t} f_B(t)dt = \hat{f}_B(\omega-\omega_0).$$

The solution of (2.1) with the forcing term (2.3) is obtained by time convolution with the "Green's" function

$$p(x,z,t) = G(x,z,t) *_t f(t).$$

Here $G(x,z,t)$ satisfies

$$\begin{aligned} -\frac{1}{c^2(x,z)}\frac{\partial^2 G(x,z,t)}{\partial t^2} + \Delta G(x,z,t) &= \delta(t)\delta(x-x_0)\delta'(z-z_0), \quad \text{for } (x,z) \in \Omega, \\ G(0,z,t) &= 0, \\ G(d,z,t) &= 0. \end{aligned} \tag{2.4}$$

Since it is easier to do multiplications than convolutions, we move to the Fourier domain and define the Fourier transform of $G(x,z,t)$ by

$$\hat{G}(x,z;\omega) = \int_{-\infty}^{\infty} G(x,z,t)e^{i\omega t}dt.$$

This is the Green's function for the Helmholtz equation

$$\begin{aligned} k^2 n^2(x,z)\hat{G}(x,z;\omega) + \Delta\hat{G}(x,z;\omega) &= \delta'(z-z_0)\delta(x-x_0) \quad \text{for } (x,z) \in \Omega, \\ \hat{G}(0,z;\omega) &= 0, \\ \hat{G}(d,z;\omega) &= 0, \end{aligned} \tag{2.5}$$

where $k = \frac{\omega}{c_0}$ is the wavenumber, and where we require $\hat{G}$ to be outgoing at $z = \pm\infty$. The pressure field in the Fourier domain is then given by

$$\hat{p}(x,z;\omega) = \hat{f}(\omega)\hat{G}(x,z;\omega). \tag{2.6}$$

2.1.2 Model of Fluctuations

We model the index of refraction as

$$n^2(x,z) = \overline{n}^2(x)(1+\epsilon\mu(x,z)), \quad (x,z) \in \Omega.$$

Here $\overline{n}(x)$ is a smooth and known profile that depends on depth only. The fluctuations are modeled as a mean zero random process μ. We suppose that μ is supported in the domain

$$\Omega' = \{[z_0, Z] \times [0,d]\},$$

and that it is statistically homogeneous in range. Its correlation function, given by

$$R(z-z', x, x') = \mathbb{E}[\mu(z,x)\mu(z',\mathbf{x}')],$$

is supposed to decay sufficiently fast as $|z-z'| \to \infty$. This means that the fluctuations decorrelate for points that are far apart. We normalize μ by

$$\frac{1}{d^2}\int_0^d \int_0^d R(0,x,x')dx\,dx' = 1,$$

and we control the magnitude of the fluctuations by a small parameter $\epsilon \ll 1$.

2.2 Derivation of the Green's Function in a Homogeneous Waveguide

In this section, we consider the Green's function in a homogeneous waveguide, with the index of refraction given by $\overline{n}(x) = 1$. The analysis can be done for any $\overline{n}(x)$, but in order to get explicit formulas for the Green's function, we take $\overline{n}(x) = 1$ and we denote the corresponding Green's function by $\hat{G}_0$.
Equation (2.5) reduces in this case to

$$\begin{aligned} k^2\hat{G}_0(x,z;\omega) + \Delta\hat{G}_0(x,z;\omega) &= \delta'(z-z_0)\delta(x-x_0) \quad \text{for } (x,z) \in \Omega, \\ \hat{G}_0(0,z;\omega) &= 0, \\ \hat{G}_0(d,z;\omega) &= 0, \end{aligned} \tag{2.7}$$

with appropriate radiation conditions at $z = \pm\infty$.

To find $\hat{G}_0$, we use the method of separation of variables. Explicitly, we expand the Green's function as

$$\hat{G}_0(x,z;\omega) = \sum_{j=1}^{\infty} \hat{\alpha}_j(z;\omega)\phi_j(x), \tag{2.8}$$

where ϕ_j are the eigenfunctions of the operator $D = -\frac{d^2}{dx^2}$, with Dirichlet conditions at $x = 0$ and $x = d$. D is positive definite and self-adjoint in $L^2[0,d]$. Its spectrum consists of an infinite number of positive eigenvalues λ_j^2, and its eigenfunctions (eigenmodes) satisfy

$$\begin{aligned} -\frac{d^2\phi_j(x)}{dx^2} &= \lambda_j^2\phi_j(x), \\ \phi_j(0) &= 0, \\ \phi_j(d) &= 0, \quad j = 1,2,... \end{aligned} \tag{2.9}$$

Here they are given by

$$\phi_j(x) = \sqrt{\frac{2}{d}}\sin(\lambda_j x), \quad \lambda_j = \frac{j\pi}{d}, \quad j = 1,2...., \tag{2.10}$$

they form a complete set in $L^2[0,d]$, and they satisfy the orthonormality relation

$$\langle \phi_l, \phi_j \rangle = \int_0^d \phi_l(x)\phi_j(x)dx = \delta_{lj}, \quad \text{for} \quad l,j = 1,2,... \tag{2.11}$$

To determine $\hat{\alpha}_j$, we use the expression for the Green's function (2.8) into equation (2.7), and recall the equations satisfied by the eigenmodes (2.9). We get

$$\sum_{j=1}^{\infty} \left[\frac{d^2\hat{\alpha}_j(z;\omega)}{dz^2} + (k^2 - \lambda_j^2)\hat{\alpha}_j(z;\omega) \right] \phi_j(x) = \delta(x - x_0)\delta'(z - z_0).$$

We then use the orthonormality of the eigenfunctions (2.11) and get a system of uncoupled ordinary differential equations (ODEs)

$$\frac{d^2\hat{\alpha}_j(z;\omega)}{dz^2} + (k^2 - \lambda_j^2)\hat{\alpha}_j(z;\omega) = \phi_j(x_0)\delta'(z - z_0), \quad \text{for} \quad j = 1,2... \tag{2.12}$$

The solution of (2.12) is given by

$$\hat{\alpha}_j(z;\omega) = \begin{cases} A_j^+ e^{i\sqrt{k^2-\lambda_j^2}(z-z_0)} + A_j^- e^{-i\sqrt{k^2-\lambda_j^2}(z-z_0)} & : \quad z > z_0 \\ B_j^+ e^{i\sqrt{k^2-\lambda_j^2}(z-z_0)} + B_j^- e^{-i\sqrt{k^2-\lambda_j^2}(z-z_0)} & : \quad z < z_0, \quad j = 1,2... \end{cases}$$

where $A^{\pm}$, $B^{\pm}$ are the mode amplitudes and where

$$\sqrt{k^2 - \lambda_j^2} = \begin{cases} \sqrt{k^2 - \lambda_j^2} & : \quad |\lambda_j| \leq k, \\ i\sqrt{\lambda_j^2 - k^2} & : \quad \text{otherwise.} \end{cases} \tag{2.13}$$

The radiation conditions for the Green's function at $z = \pm\infty$ imply that

$$A_j^- = B_j^+ = 0, \quad j = 1,2....$$

At $z = z_0$, we have the jump conditions:

$$\left[\frac{d\hat{\alpha}_j}{dz} \right] = 0, \tag{2.14}$$

and

$$[\hat{\alpha}_j] = \phi_j(x_0). \tag{2.15}$$

Using those, we obtain

$$A_j^+ = -B_j^-,$$

and

$$A_j^+ = \frac{\phi_j(x_0)}{2}.$$

Putting everything together, we get

$$\hat{G}_0(x,z;\omega) = \sum_{j=1}^{\infty} \frac{\phi(x_0)}{2}\phi_j(x)\big(e^{i\sqrt{k^2-\lambda_j^2}(z-z_0)}\chi_{(z_0,\infty)}(z) + e^{-i\sqrt{k^2-\lambda_j^2}(z-z_0)}\chi_{(-\infty,z_0)}(z)\big), \tag{2.16}$$

and in the time domain

$$\begin{aligned} G_0(x,z,t) = \int d\omega \sum_{j=1}^{\infty} \frac{\phi(x_0)}{2}\phi_j(x)\big(e^{i[\sqrt{k^2-\lambda_j^2}(z-z_0)-\omega t]}\chi_{(z_0,\infty)}(z) \\ + e^{-i[\sqrt{k^2-\lambda_j^2}(z-z_0)+\omega t]}\chi_{(-\infty,z_0)}(z)\big). \end{aligned} \tag{2.17}$$

Note here that for j satisfying

$$|\lambda_j| \leq k = \frac{\omega}{c_0}, \quad i.e. \quad \text{for} \quad j \leq N(\omega) = \frac{\omega d}{\pi c_0}, \tag{2.18}$$

we have $\sqrt{k^2-\lambda_j^2} \in \mathbb{R}$. In this case, the modal wave numbers are defined as

$$\beta_j(\omega) = \sqrt{(\frac{\omega}{c_0})^2 - \lambda_j^2} \tag{2.19}$$

and they correspond to propagating modes. These move to the right of the source in (z_0,∞), or to the left in $(-\infty,z_0)$, with constant amplitudes and group velocity $c_0\{\frac{\partial\beta_j(\omega)}{\partial\omega}\}^{-1}$.

The number of these modes is an increasing function of depth and frequency as seen in (2.18). For $j > N(\omega)$, $\sqrt{k^2-\lambda_j^2}$ are imaginary and we define

$$\beta_j(\omega) = \sqrt{\lambda_j^2 - (\frac{\omega}{c_0})^2}. \tag{2.20}$$

These correspond to evanescent modes that decay exponentially in range.

Distinguishing between the propagating and evanescent modes, the homogeneous Green's function is expressed as

$$\hat{G}_0(x,z;\omega) = \sum_{j=1}^{N(\omega)} \frac{\phi(x_0)}{2}\phi_j(x)\big(e^{i\beta_j(\omega)(z-z_0)}\chi_{(z_0,\infty)}(z) + e^{-i\beta_j(\omega)(z-z_0)}\chi_{(-\infty,z_0)}(z)\big) + \sum_{j>N(\omega)} \frac{\phi(x_0)}{2}\phi_j(x)\big(e^{-\beta_j(\omega)(z-z_0)}\chi_{(z_0,\infty)}(z) + e^{\beta_j(\omega)(z-z_0)}\chi_{(-\infty,z_0)}(z)\big). \tag{2.21}$$

By neglecting the evanescent modes for sufficiently large $z - z_0$, $\hat{G}_0$ can be approximated by

$$\hat{G}_0(x,z;\omega) \approx \sum_{j=1}^{N(\omega)} \frac{\phi(x_0)}{2}\phi_j(x)\big(e^{i\beta_j(\omega)(z-z_0)}\chi_{(z_0,\infty)}(z) + e^{-i\beta_j(\omega)(z-z_0)}\chi_{(-\infty,z_0)}(z)\big). \tag{2.22}$$

2.3 The Green's Function in a Random Waveguide

We now consider the Green's function in a waveguide with a randomly fluctuating index of refraction

$$n^2(x) = 1 + \epsilon\mu(x,z).$$

We follow the analysis done in [13]. As in the previous section, $\hat{G}$ is expanded in terms of the eigenfunctions $\hat{\phi}_j$ given by (2.10), but the coefficients in the expansion are now random, and they satisfy a system of coupled ODEs. The coupling is due to the fluctuations, and it is responsible for the transfer of energy between the propagating and evanescent modes.

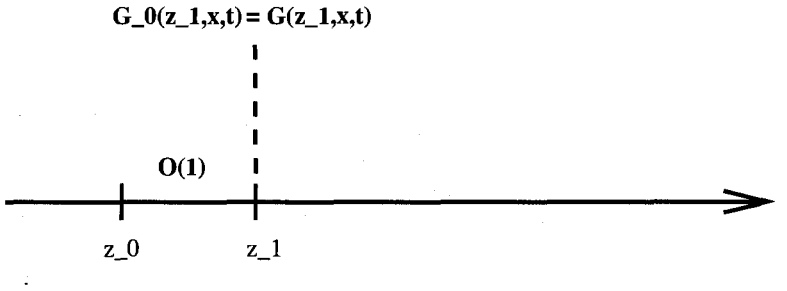

Figure 2.2: Matching of G to G_0 at $z = z_1$

2.3.1 The Stochastic ODEs for the Mode Amplitudes

The outgoing Green's function in the random waveguide satisfies

$$\begin{aligned} k^2(1+\epsilon\mu(x,z))\hat{G}(x,z;\omega) + \Delta\hat{G}(x,z;\omega) = 0, \quad \text{for } (x,z) \in \Omega \quad s.t. \quad z > z_1 \\ \hat{G}(0,z,\omega) = 0, \\ \hat{G}(d,z;\omega) = 0. \end{aligned} \tag{2.23}$$

We account for the source term by matching the Green's function to the homogeneous Green's function at z_1

$$G(z = z_1, x, t) = G_0(z = z_1, x, t). \tag{2.24}$$

This can be done because $z_1 - z_0 = O(1)$, and the small fluctuations do not have an effect over such distances.

The Green's function is now expanded as follows

$$\hat{G}(x,z;\omega) = \sum_{j=1}^{N(\omega)} \phi_j(x)\hat{\gamma}_j(z;\omega) + \sum_{j=N(\omega)+1}^{\infty} \phi_j(x)\hat{q}_j(z;\omega). \tag{2.25}$$

Here the propagating modes correspond to $j \leq N(\omega)$ and the evanescent ones correspond to $j > N(\omega)$. $\hat{\gamma}_j$ denotes the coefficient of the j^{th} propagating mode and $\hat{q}_j$ denotes the coefficient of the j^{th} evanescent mode. Each propagating mode is further decomposed as

$$\hat{\gamma}_j(z;\omega) = \frac{1}{\sqrt{\beta_j(\omega)}}\left(\hat{a}_j(z;\omega)e^{i\beta_j(\omega)z} + \hat{b}_j(z;\omega)e^{-i\beta_j(\omega)(z)}\right), \tag{2.26}$$

with $\hat{a}_j$ and $\hat{b}_j$ denoting the random complex "amplitudes" of the j^{th} forward and backward moving modes respectively. These are functions of range, and in order to define them uniquely, an additional relation is prescribed

$$\frac{d\hat{a}_j(z;\omega)}{dz}e^{i\beta_j(\omega)(z)} + \frac{d\hat{b}_j(z;\omega)}{dz}e^{-i\beta_j(\omega)(z)} = 0. \tag{2.27}$$

We shall study $\hat{a}$ and $\hat{b}$ at fixed frequency, so from now on, we drop ω from the notation.

A system of equations for $\hat{a}_j$ and $\hat{b}_j$ is now obtained using (2.25), (2.26), (2.27) in equation (2.23). From the orthonormality of the eigenmodes (2.11), we get the following system of coupled differential equations for the propagating and evanescent mode amplitudes

$$\begin{aligned}\frac{d\hat{a}_j}{dz}(z) &= \frac{i\epsilon k^2}{2}\sum_{l=1}^{N}\frac{C_{jl}(z)}{\sqrt{\beta_j\beta_l}}\left[\hat{a}_l(z)e^{i(\beta_l-\beta_j)(z)} + \hat{b}_l(z)e^{-i(\beta_l+\beta_j)(z)}\right] \\ &\quad + \frac{i\epsilon k^2}{2\sqrt{\beta_j}}\sum_{l>N}C_{jl}(z)\hat{q}_l(z)e^{-i\beta_j(z)}, \end{aligned}\tag{2.28}$$

$$\begin{aligned}\frac{d\hat{b}_j}{dz}(z) &= -\frac{i\epsilon k^2}{2}\sum_{l=1}^{N}\frac{C_{jl}(z)}{\sqrt{\beta_j\beta_l}}\left[\hat{a}_l(z)e^{i(\beta_l+\beta_j)z} + \hat{b}_l(z)e^{-i(\beta_j-\beta_l)z}\right] \\ &\quad - \frac{i\epsilon k^2}{2\sqrt{\beta_j}}\sum_{l>N}C_{jl}(z)\hat{q}_l(z)e^{i\beta_j(z)}, \quad j = 1,..N, \end{aligned}\tag{2.29}$$

$$\frac{d^2\hat{q}_j}{dz^2}(z) - \beta_j^2\hat{q}_j(z) + \epsilon g_j(z) = 0, \quad j \geq N+1. \tag{2.30}$$

Here $C_{jl}(z)$ is the symmetric matrix with entries

$$C_{jl}(z) = \int_0^d \phi_j(x)\phi_l(x)\mu(z,x)dx, \tag{2.31}$$

and

$$g_j(z) = k^2\sum_{l>N}C_{jl}(z)\hat{q}_l(z) + k^2\sum_{1}^{N}\frac{C_{jl}(z)}{\sqrt{\beta_l}}\left(\hat{a}_j e^{i\beta_j(z)} + \hat{b}_j e^{-i\beta_j(z)}\right). \tag{2.32}$$

The right going mode amplitudes satisfy the initial condition

$$\hat{a}_j(z_1) = \hat{a}_{j,0}, \tag{2.33}$$

where $\hat{a}_{j,0}$ are obtained by the matching condition (2.24) (an explicit expression for $\hat{a}_{j,0}$ will be given later, after the forward scattering approximation). The left going amplitudes satisfy

$$\hat{b}_j(Z) = 0, \tag{2.34}$$

This states that no wave is incoming from the right. The evanescent modes decay exponentially as range increases

$$\lim_{z\to\pm\infty} \hat{q}_j(z) = 0. \tag{2.35}$$

2.3.2 Evanescent Modes in Terms of Propagating Modes

The coefficients of the evanescent modes $\hat{q}_j$ are now eliminated from the equations of $\hat{a}_j$ and $\hat{b}_j$ (2.28) and (2.29). Notice first that the solution of (2.30) with the decay condition (2.35) is of the form

$$\hat{q}_j(z) = \frac{\epsilon}{2\beta_j}\int_{-\infty}^{\infty} g_j(z+s)e^{-\beta_j|s|}ds. \tag{2.36}$$

This is not an explicit formula for $\hat{q}_j$ because g_j depends on $\hat{q}_j$, as seen in equation (2.32). Using the latter, we can rewrite (2.36) as a linear system

$$(I - \epsilon\Psi)\hat{q} = \epsilon\tilde{q},$$

where Ψ is the integral operator

$$(\Psi\hat{q})_j(z) = \frac{k^2}{2\beta_j}\sum_{l>N}\int_{-\infty}^{\infty} C_{jl}(z+s)\hat{q}_l e^{-\beta_j|s|}ds, \tag{2.37}$$

and

$$\tilde{q}_j(z) = \frac{k^2}{2\beta_j}\sum_{1\le N}\int_{-\infty}^{\infty}\frac{C_{jl}(z+s)}{\sqrt{\beta_l}}\left(\hat{a}_l(z+s)e^{i\beta_l(z+s)} + \hat{b}_l(z+s)e^{-i\beta_l(z+s)}\right)e^{-\beta_j|s|}ds, \tag{2.38}$$

for $j > N$.

It is shown in [13] that Ψ is a bounded operator, so we can write

$$(I - \epsilon\Psi)^{-1} = I + \epsilon\Psi + O(\epsilon^2),$$

using $\epsilon \ll 1$, and obtain

$$\hat{q}_j(z) = \frac{\epsilon k^2}{2\beta_j} \sum_{1\le N} \int_{-\infty}^{\infty} \frac{C_{jl}(z+s)}{\sqrt{\beta_l}} \left(\hat{a}_l(z+s)e^{i\beta_l(z+s)} + \hat{b}_l(z+s)e^{-i\beta_l(z+s)}\right) e^{-\beta_j|s|} ds + O(\epsilon^2), j > N$$

Note that due to the presence of the exponentially decaying term $e^{-\beta_j|s|}$, we can confine s to an interval of $O(1)$ around z. In this case, we have from (2.28), (2.29)

$$\hat{a}_j(z+s) = \hat{a}_j(z) + O(\epsilon), \quad \hat{b}_j(z+s) = \hat{b}_j(z) + O(\epsilon),$$

and using this fact in the expression for $\hat{q}$, we get

$$\hat{q}_j(z) = \frac{\epsilon k^2}{2\beta_j} \sum_{1\le N} \int_{-\infty}^{\infty} \frac{C_{jl}(z+s)}{\sqrt{\beta_l}} \left(\hat{a}_l(z)e^{i\beta_l(z+s)} + \hat{b}_l(z)e^{-i\beta_l(z+s)}\right) e^{-\beta_j|s|} ds + O(\epsilon^2), \quad j > N. \tag{2.39}$$

2.3.3 Equations for the Propagating Mode Amplitudes

This result is now used in the system (2.28),(2.29), and (2.30). The evanescent modes are eliminated and the propagating mode amplitudes satisfy

$$\frac{d\hat{\mathbf{a}}}{dz}(z) = \epsilon[\mathbf{H}^{(aa)}(z)\hat{\mathbf{a}}(z) + \mathbf{H}^{(ab)}(z)\hat{\mathbf{b}}(z)] + \epsilon^2[\mathbf{G}^{(aa)}(z)\hat{\mathbf{a}}(z) + \mathbf{G}^{(ab)}(z)\hat{\mathbf{b}}(z)] + O(\epsilon^3) \tag{2.40}$$

$$\frac{d\hat{\mathbf{b}}}{dz}(z) = \epsilon[\mathbf{H}^{(ba)}(z)\hat{\mathbf{a}}(z) + \mathbf{H}^{(bb)}(z)\hat{\mathbf{b}}(z)] + \epsilon^2[\mathbf{G}^{(ba)}(z)\hat{\mathbf{a}}(z) + \mathbf{G}^{(bb)}(z)\hat{\mathbf{b}}(z)] + O(\epsilon^3), \tag{2.41}$$

where $\hat{\mathbf{a}}$ and $\hat{\mathbf{b}}$ are vectors with entries

$$(\hat{\mathbf{a}})_j(z) = \hat{a}_j(z), \quad (\hat{\mathbf{b}})_j(z) = \hat{b}_j(z),$$

and $\mathbf{H}^{(\cdot)}$, $\mathbf{G}^{(\cdot)}$ are matrices with entries

$$H_{jl}^{(aa)}(z) = \frac{ik^2}{2} \frac{C_{jl}(z)}{\sqrt{\beta_j\beta_l}} e^{i(\beta_l-\beta_j)(z)}, \tag{2.42}$$

$$H_{jl}^{(ab)}(z) = \frac{ik^2}{2} \frac{C_{jl}(z)}{\sqrt{\beta_j\beta_l}} e^{-i(\beta_l+\beta_j)(z)}, \tag{2.43}$$

$$H_{jl}^{(ba)}(z) = -\frac{ik^2}{2}\frac{C_{jl}(z)}{\sqrt{\beta_j\beta_l}}e^{i(\beta_l+\beta_j)(z)}, \tag{2.44}$$

$$H_{jl}^{(bb)}(z) = -\frac{ik^2}{2}\frac{C_{jl}(z)}{\sqrt{\beta_j\beta_l}}e^{i(\beta_j-\beta_l)(z)}, \tag{2.45}$$

$$G_{jl}^{(aa)}(z) = \frac{ik^4}{4}\sum_{l'>N}\int_{-\infty}^{\infty}\frac{C_{jl'}(z)C_{ll'}(z+s)}{\sqrt{\beta_j\beta_{l'}^2\beta_l}}e^{i\beta_l(z+s)-i\beta_j(z)-\beta_{l'}|s|}ds, \tag{2.46}$$

$$G_{jl}^{(ab)}(z) = \frac{ik^4}{4}\sum_{l'>N}\int_{-\infty}^{\infty}\frac{C_{jl'}(z)C_{ll'}(z+s)}{\sqrt{\beta_j\beta_{l'}^2\beta_l}}e^{-i\beta_l(z+s)-i\beta_j(z)-\beta_{l'}|s|}ds, \tag{2.47}$$

$$G_{jl}^{(ba)}(z) = -\frac{ik^4}{4}\sum_{l'>N}\int_{-\infty}^{\infty}\frac{C_{jl'}(z)C_{ll'}(z+s)}{\sqrt{\beta_j\beta_{l'}^2\beta_l}}e^{i\beta_l(z+s)+i\beta_j(z)-\beta_{l'}|s|}ds \tag{2.48}$$

and

$$G_{jl}^{(ba)}(z) = -\frac{ik^4}{4}\sum_{l'>N}\int_{-\infty}^{\infty}\frac{C_{jl'}(z)C_{ll'}(z+s)}{\sqrt{\beta_j\beta_{l'}^2\beta_l}}e^{-i\beta_l(z+s)+i\beta_j(z)-\beta_{l'}|s|}ds. \tag{2.49}$$

for $j = 1, 2, ..N$.

At $z = z_1$, we have $\hat{\mathbf{a}}(z_1) = \hat{\mathbf{a}}_0$ and at $z = Z$ we have $\hat{\mathbf{b}}(Z) = \mathbf{0}$. Note that the coupling with the evanescent modes is done through the matrices $\mathbf{G}^{(.)}$.

2.4 Asymptotic Analysis of the Coupled Stochastic ODEs

In this section, the system of stochastic ODEs for the propagating mode amplitudes is analyzed, in the limit $\epsilon \to 0$. Since the fluctuations are weak, of $O(\epsilon)$, their effect becomes visible when the waves propagate over very long distances. From equations (2.40) and (2.41) we would expect a propagation distance of $O(\frac{1}{\epsilon})$ to see $O(1)$ variation in the amplitudes. However, if we look at the coherent fields $\mathbb{E}[\hat{\mathbf{a}}]$ and

$\mathbb{E}[\hat{\mathbf{b}}]$, the $O(\frac{1}{\epsilon})$ terms in the right hand side of (2.40) and (2.41) have zero mean. This is why the right scaling for this problem is $Z = O(\frac{1}{\epsilon^2})$.

So let $Z = \frac{L}{\epsilon^2}$, where $L = O(1)$, and introduce the notation

$$\hat{\mathbf{a}}^\epsilon(z) = \hat{\mathbf{a}}(\frac{z}{\epsilon^2}), \quad \hat{\mathbf{b}}^\epsilon(z) = \hat{\mathbf{b}}(\frac{z}{\epsilon^2}).$$

We get from (2.40) and (2.41) the following

$$\frac{d}{dz}\begin{pmatrix} \hat{\mathbf{a}}^\epsilon \\ \hat{\mathbf{b}}^\epsilon \end{pmatrix} = \mathbf{H}^\epsilon(z)\begin{pmatrix} \hat{\mathbf{a}}^\epsilon \\ \hat{\mathbf{b}}^\epsilon \end{pmatrix}, \tag{2.50}$$

where

$$\mathbf{H}^{(\epsilon)}(z) = \frac{1}{\epsilon}\begin{pmatrix} \mathbf{H}^{(aa)}(\frac{z}{\epsilon^2}) & \mathbf{H}^{(ab)}(\frac{z}{\epsilon^2}) \\ \mathbf{H}^{(ba)}(\frac{z}{\epsilon^2}) & \mathbf{H}^{(bb)}(\frac{z}{\epsilon^2}) \end{pmatrix} + \begin{pmatrix} \mathbf{G}^{(aa)}(\frac{z}{\epsilon^2}) & \mathbf{G}^{(ab)}(\frac{z}{\epsilon^2}) \\ \mathbf{G}^{(ba)}(\frac{z}{\epsilon^2}) & \mathbf{G}^{(bb)}(\frac{z}{\epsilon^2}) \end{pmatrix}.$$

The initial conditions are

$$\hat{\mathbf{a}}^\epsilon(\epsilon^2 z_1) = \hat{\mathbf{a}}_0,$$

and the end condition is

$$\hat{\mathbf{b}}^\epsilon(z = L) = \mathbf{0}.$$

The solution of (2.50) can be expressed conveniently using propagator matrices as

$$\begin{pmatrix} \hat{\mathbf{a}}^\epsilon(z) \\ \hat{\mathbf{b}}^\epsilon(z) \end{pmatrix} = \mathbf{P}^\epsilon(z)\begin{pmatrix} \hat{\mathbf{a}}^\epsilon{}_0 \\ \mathbf{0} \end{pmatrix}. \tag{2.51}$$

Here $\mathbf{P}^\epsilon$ is a random matrix solving

$$\frac{d}{dz}\mathbf{P}^\epsilon = \mathbf{H}^\epsilon(z)\mathbf{P}^\epsilon, \quad \text{for} \quad \epsilon^2 z_1 \le z \le L,$$

with initial condition $\mathbf{P}^\epsilon(z = \epsilon^2 z_1) = \mathbf{I}$, where $\mathbf{I}$ is the identity matrix.

It can be easily checked that the propagator has the form

$$\mathbf{P}^\epsilon(z) = \begin{pmatrix} \mathbf{P}^\epsilon_{(aa)}(z) & \mathbf{P}^\epsilon_{(ab)}(z) \\ \overline{\mathbf{P}^\epsilon_{(ab)}(z)} & \overline{\mathbf{P}^\epsilon_{(aa)}(z)} \end{pmatrix}.$$

since the matrices $\mathbf{H}^{(\cdot,\cdot)}$ and $\mathbf{G}^{(\cdot,\cdot)}$ satisfy

$$\mathbf{H}^{aa}(z) = \overline{\mathbf{H}^{bb}(z)}, \quad \mathbf{H}^{ab}(z) = \overline{\mathbf{H}^{ba}(z)},$$

$$\mathbf{G}^{aa}(z) = \overline{\mathbf{G}^{bb}(z)}, \quad \mathbf{G}^{ab}(z) = \overline{\mathbf{G}^{ba}(z)}.$$

Note here that the matrix $\mathbf{P}^{\epsilon}_{(aa)}(z)$ gives the coupling among the forward modes, whereas $\mathbf{P}^{\epsilon}_{(ab)}(z)$ is responsible for coupling the forward and backward modes.

2.4.1 The Forward Scattering Approximation

The forward scattering approximation consists of neglecting the backward propagating modes $\hat{b}^{\epsilon}_j(z)$, in the limit $\epsilon \to 0$. To get an idea why it is reasonable to do so, we compare the terms responsible for the coupling among the forward modes, to those responsible for the coupling between the backwards and forward modes.

In the limit $\epsilon \to 0$, the coupling between the forward and backward modes is done through the coefficients

$$\int_{-\infty}^{\infty} \mathbb{E}[C_{jl}(0)C_{jl}(z)] \cos\left((\beta_j + \beta_l)z\right)dz, \;\; j,l = 1,2...N, \tag{2.52}$$

whereas the coupling between the forward modes is done through

$$\int_{-\infty}^{\infty} \mathbb{E}[C_{jl}(0)C_{jl}(z)] \cos\left((\beta_j - \beta_l)z\right)dz, \;\; j,l = 1,2...N. \tag{2.53}$$

This is clear if we recall that the phase factors in $H_{(ab)}(z)$ are $\pm(\beta_j + \beta_l)z$, and in $H_{(aa)}(z)$, they are $\pm(\beta_j - \beta_l)z$.

The coefficients given by (2.52) and (2.53) are just the Fourier modes of the autocorrelation function of C_{jl} given by

$$\mathbb{E}[C_{jl}(0)C_{jl}(z)] = \int_0^d \int_0^d \phi_j(x)\phi_j(x)\phi_j(x')\phi_l(x')R(z,x,x')dxdx'.$$

If R is smooth enough in z, then the coefficients in (2.52) are small in comparison with the coefficients in (2.53). Under that assumption, we can make the approximation

$$\int_{-\infty}^{\infty} \mathbb{E}[C_{jl}(0)C_{jl}(z)] \cos\left((\beta_j + \beta_l)z\right)dz \approx 0, \;\; j,l = 1,2\ldots N \tag{2.54}$$

If we also take into consideration the initial condition $\mathbf{P}^{(ab)}(z = \epsilon^2 z_1) = \mathbf{0}$, we conclude that the O.D.E's for the forward and backward modes decouple in the limit $\epsilon \to 0$. This is the forward scattering approximation that consists of dropping $\mathbf{b}^\epsilon$ (See a discussion on the forward scattering approximation in underwater acoustics in [28]).

The Green's function is now given by

$$\hat{G}^\epsilon(x, z; \omega) \approx \sum_{j=1}^{N} \phi_j(x) \frac{\hat{a}_j^\epsilon(z)}{\sqrt{\beta_j}} e^{i\beta_j(\frac{z}{\epsilon^2})}, \tag{2.55}$$

where the modes amplitudes satisfy

$$\frac{d\hat{\mathbf{a}}^\epsilon}{dz} = [\frac{1}{\epsilon}\mathbf{H}^{(aa)}(\frac{z}{\epsilon^2}) + \mathbf{G}^{(aa)}(\frac{z}{\epsilon^2})]\hat{\mathbf{a}}^\epsilon, \quad \epsilon^2 z_1 \leq z \leq L \tag{2.56}$$

with

$$\hat{a}_j^\epsilon(\epsilon^2 z_1) = \hat{a}_{j,0}, \quad j = 1, 2 \ldots N.$$

We now obtain $\hat{a}_{j,0}$ from the matching condition (2.24), that is,

$$\sum_{j=1}^{N} \frac{\phi(x_0)}{2} \phi_j(x) e^{i\beta_j(z_1 - z_0)} = \sum_{j=1}^{N} \phi_j(x) \frac{\hat{a}^\epsilon(\epsilon^2 z_1)}{\sqrt{\beta_j}} e^{i\beta_j z_1} = \sum_{j=1}^{N} \phi_j(x) \frac{\hat{a}_{j,0}}{\sqrt{\beta_j}} e^{i\beta_j z_1}.$$

So we have

$$\hat{a}_{j,0} = \frac{\phi_j(x_0)}{2} \sqrt{\beta_j} e^{-i\beta_j z_0}, \quad j = 1, ..N. \tag{2.57}$$

2.4.2 Application of the Diffusion Limit to the Stochastic System of ODEs

Under the scaling described above, the diffusion limit as $\epsilon \to 0$ is taken. This limit is analyzed by Kashminski in [19] as well as Papanicolaou in [25]. We give the statement of the diffusion limit in the appendix. Here, we state the following limit result concerning the mode amplitudes, which is given in [13]

Proposition 1. *The complex mode amplitudes* $(\hat{a}_j^\epsilon(z))_{j=1,2..N}$ *converge in distribution as* $\epsilon \to 0$, *to a diffusion process* $(\hat{a}_j(z))_{j=1,2..N}$, *with infinitesimal generator* $\mathcal{L}$ *given*

by

$$\mathcal{L} = \frac{1}{4}\sum_{j\neq l}\Gamma^{(c)}_{jl}(A_{jl}\overline{A}_{jl}+\overline{A}_{jl}A_{jl})+\frac{1}{2}\sum_{j,l}\Gamma^{(1)}_{jl}A_{jj}\bar{A}_{ll}+\frac{i}{4}\sum_{j\neq l}\Gamma^{(s)}_{jl}(A_{ll}-A_{jj})+i\sum_{j}\kappa_j A_{jj}, \tag{2.58}$$

where

$$A_{jl} = \hat{a}_j\frac{\partial}{\partial\hat{a}_l} - \overline{\hat{a}_l}\frac{\partial}{\partial\overline{\hat{a}_j}} = -\overline{A_{lj}}.$$

The coefficients $\Gamma^{(c)}_{jl}$, $\Gamma^{(s)}_{jl}$ *and* $\Gamma^{(1)}_{jl}$ *are given by:*

$$\Gamma^{(c)}_{jl} = \frac{k^4\gamma^{(c)}_{jl}}{4\beta_j\beta_l} \text{ if } j\neq l, \tag{2.59}$$

$$\Gamma^{(c)}_{jj} = -\sum_{n\neq j}\Gamma^{(c)}_{jn}, \tag{2.60}$$

$$\gamma^{(c)}_{jl} = \int_{-\infty}^{\infty}\cos\left((\beta_j-\beta_l)z\right)\mathbb{E}[C_{jl}(0)C_{jl}(z)]dz, \tag{2.61}$$

$$\Gamma^{(s)}_{jl} = \frac{k^4\gamma^{(s)}_{jl}}{4\beta_j\beta_l} \text{ if } j\neq l, \tag{2.62}$$

$$\Gamma^{(s)}_{jj} = -\sum_{n\neq j}\Gamma^{(s)}_{jn}, \tag{2.63}$$

$$\gamma^{(s)}_{jl} = 2\int_{0}^{\infty}\sin\left((\beta_j-\beta_l)z\right)\mathbb{E}[C_{jl}(0)C_{jl}(z)]dz, \tag{2.64}$$

$$\Gamma^{(1)}_{jl} = \frac{k^4\gamma^{(1)}_{jl}}{4\beta_j\beta_l} \text{ for all } j,l, \tag{2.65}$$

$$\gamma^{(1)}_{jl} = \int_{-\infty}^{\infty}\mathbb{E}[C_{jj}(0)C_{ll}(z)]dz, \tag{2.66}$$

and

$$\kappa_j = \sum_{l'>N}\frac{k^4}{4\beta_{l'}\beta_j}\int_{-\infty}^{\infty}\cos\left(\beta_j s\right)e^{-\beta_{l'}|s|}\mathbb{E}[C_{jl'}(0)C_{jl'}(s)]ds, \tag{2.67}$$

The details of the computation of the generator are left to the Appendix. Here, we give the expressions for the first and second moments of the modes amplitudes given in [13].

2.4.3 Moments

Proposition 2. *The expected value of the modes amplitudes* $\mathbb{E}[\hat{a}_j^\epsilon(z)]$ *converge as* $\epsilon \to 0$ *to*

$$\mathbb{E}[\hat{a}_j(z)] = \exp\left(\frac{\Gamma_{jj}^{(c)} z}{2} - \frac{\Gamma_{jj}^{(1)} z}{2} + i\frac{\Gamma_{jj}^{(s)} z}{2} + i\kappa_j z\right)\hat{a}_{j,0},$$

where $\Gamma_{jj}^{(c)}$, $\Gamma_{jj}^{(1)}$, $\Gamma_{jj}^{(s)}$, *and* κ_j *are given respectively by* (2.60), (2.65), (2.60) *and* (2.67).

Notice that $\Gamma_{jj}^{(c)}$ is negative and that $\Gamma_{jj}^{(1)}$ is nonnegative because it is proportional to the power spectral density of the stationary random process C_{jj} at 0-frequency [26]. The coefficient $[\Gamma_{jj}^{(c)} - \Gamma_{jj}^{(1)}]/2$ is therefore negative and it is responsible for damping the modes. This damping depends on the mode number, the frequency and range. The coefficients κ_j and $\Gamma_{jj}^{(s)}$ introduce a phase change that also depends on mode number, frequency and range.

Proposition 3. *The second moments of the modes amplitudes* $\mathbb{E}[\hat{a}_j^\epsilon(z)\overline{\hat{a}^\epsilon}_l(z)]$ *converge as* $\epsilon \to 0$ *to*

$$\mathbb{E}[\hat{a}_j(z)\overline{\hat{a}_l(z)}] = e^{\mathcal{Q}_{jl}z}\hat{a}_{j,0}\overline{\hat{a}_{l,0}} \quad \text{if} \quad j \neq l, \tag{2.68}$$

$$\mathbb{E}[|\hat{a}_j(z)|^2] = \mathcal{P}_j^{(1)}(z) \quad \text{if} \quad j = l, \tag{2.69}$$

where

$$\mathcal{Q}_{jl} = \frac{\Gamma_{jj}^{(c)} + \Gamma_{ll}^{(c)}}{2} - \frac{\Gamma_{jj}^{(1)} + \Gamma_{ll}^{(1)} - 2\Gamma_{jl}^{(1)}}{2} + i\frac{\Gamma_{jj}^{(s)} - \Gamma_{ll}^{(s)}}{2} + i[\kappa_j - \kappa_l], \tag{2.70}$$

and where $\mathcal{P}_j^{(1)}$ *solves*

$$\frac{\partial \mathcal{P}_j^{(1)}}{\partial z} = \sum_{n \neq j} \Gamma_{jn}^{(1)}\left(\mathcal{P}_n^{(1)} - \mathcal{P}_j^{(1)}\right), \tag{2.71}$$

starting from $\mathcal{P}_j^{(1)}(0) = |\hat{a}_{j,0}|^2$.

Chapter 3

Imaging of a Point Source in a Waveguide

3.1 Migration Imaging

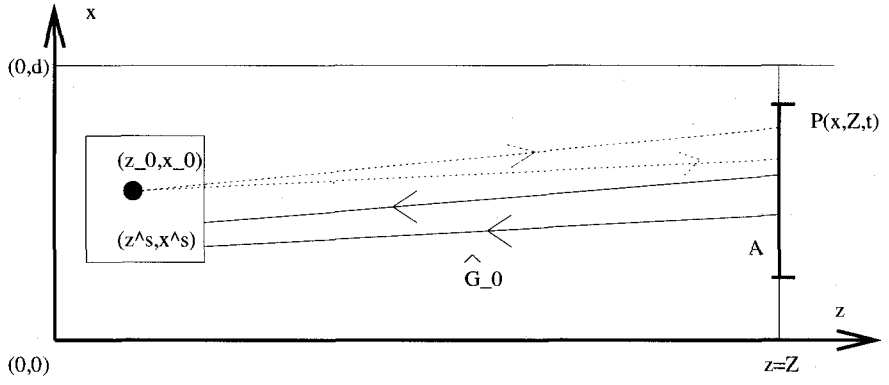

Figure 3.1: Setup for the derivation of the migration formula in the waveguide

We now consider imaging a point source located at $(x_0, z_0) \in \Omega$. This source emits a pulse $f(t)$, and at a vertical array $\mathcal{A}$ situated at $z = Z$, we record the time traces of the pressure field in a time window $[t_0, t_f]$.

To find the location of the source, we back propagate the pressure field from the

array receivers $x \in \mathcal{A}$ in a homogeneous waveguide, to a search point (x^s, z^s) where the image is formed. We integrate over the receivers positions in $\mathcal{A}$ and form the migration imaging function

$$\mathcal{I}^{(MIG)}(x^s, z^s) = \int\int_{x\in\mathcal{A}} \hat{p}(x, Z; \omega, x_0, z_0)\overline{\hat{G}_0(x^s, z^s; \omega, x, Z)}dx\, d\omega \tag{3.1}$$

We want to study the properties of this imaging function in the random waveguide and compare it to the homogeneous waveguide. According to the scaling for propagation in the random waveguide, used in section 2.4, we take $Z = \frac{L}{\epsilon^2}$, where $\epsilon \ll 1$ and $L = O(1)$.

3.2 Imaging in a Homogeneous Waveguide

If we assume that the waveguide is homogeneous, then the pressure field at the array is given by equations (2.6) and (2.22), that is, we have

$$\hat{p}(x, Z; \omega, x_0, z_0) \approx \frac{\hat{f}(\omega)}{2} \sum_{j=1}^{N(\omega)} \phi(x_0)\phi(x)e^{i\beta_j(\omega)(Z-z_0)},$$

with $\phi(x) = \sqrt{\frac{2}{d}}\sin(\lambda_j x)$, $\lambda_j = \frac{j\pi}{d}$, $\beta_j = \sqrt{(\frac{\omega}{c_0})^2 - \lambda_j^2}$ and $N(\omega) = \frac{d\omega}{c_0\pi}$.
Here we neglect the evanescent modes which decay exponentially in range, since the propagation distance is large. The migration function is then given by

$$\mathcal{I}^{MIG}(x^s, z^s) \approx \int \frac{\hat{f}(\omega)}{4} \sum_{l,j}^{N(\omega)} M_{lj}e^{i(\beta_j(\omega)-\beta_l(\omega))Z}e^{i\beta_l(\omega)z^s}e^{-i\beta_j(\omega)z_0}\phi_l(x^s)\phi_j(x_0)d\omega, \tag{3.2}$$

where M is the matrix whose entries are

$$M_{lj} = \int_0^d \chi_{\mathcal{A}}(x)\phi_l(x)\phi_j(x)dx. \tag{3.3}$$

We can study focusing in the cross range direction (depth x) by fixing z^s at the source location z_0. In the simple case where the array spans the entire depth (full

aperture), then $M_{l,j} = \delta_{lj}$, since the eigenfunctions are orthonormal. The migration function simplifies to

$$\mathcal{I}^{MIG}(x^s, z^s) \approx \int \frac{\hat{f}(\omega)}{2d} \sum_j^{N(\omega)} e^{i\beta_j(\omega)(z^s - z_0)} \sin(\lambda_j x^s) \sin(\lambda_j x_0) d\omega.$$

and the cross range focusing profile is given by the function

$$H(x^s) = \int \frac{\hat{f}(\omega)}{2d} \sum_j^{N(\omega)} \sin(\frac{j\pi}{d} x^s) \sin(\frac{j\pi}{d} x_0) d\omega,$$

Note that it depends on the number of modes and on the pulse shape.

3.3 Imaging in a Cluttered Waveguide

Recalling the equations for the pressure field and the mode amplitudes in the random waveguide (2.55) and (2.56), we see that the pressure field measured at $\frac{L}{\epsilon^2}$, is

$$\hat{p}(x, \frac{L}{\epsilon^2}; \omega) = \hat{f}(\omega)\hat{G}(x, \frac{L}{\epsilon^2}; \omega, z_0, x_0) \approx \hat{f}(\omega) \sum_{j=1}^{N(\omega)} \frac{\hat{a}_j^{\epsilon}(L; \omega)}{\sqrt{\beta_j(\omega)}} \phi_j(x) e^{i\beta_j(\omega)(\frac{L}{\epsilon^2})}, \quad x \in A,$$

where $\hat{a}_j^{\epsilon}$ are the random mode amplitudes, solutions of (2.56). Back-propagating this field in a homogeneous waveguide gives

$$\mathcal{I}^{MIG}(x^s, z^s) \approx \int \frac{\hat{f}(\omega)}{2} \sum_{l,j}^{N(\omega)} M_{lj} \frac{\hat{a}_j^{\epsilon}(L; \omega)}{\sqrt{\beta_j(\omega)}} e^{i(\beta_j(\omega) - \beta_l(\omega))\frac{L}{\epsilon^2}} e^{i\beta_l(\omega) z^s} \phi_l(x^s) d\omega, \qquad (3.4)$$

with M_{lj} given by (3.3).

We want to study the focusing properties of (3.4). This is a random function so we shall look at its moments. The first moment is the expectation of (3.4), given by the expected or coherent pressure field at the array. Using Proposition 2, we see that the expectation of (3.4) is

$$\mathbb{E}[\mathcal{I}^{MIG}(x^s, z^s)] \approx \int \frac{\hat{f}(\omega)}{4} \sum_{l,j}^{N(\omega)} M_{lj}\, e^{i(\beta_j(\omega) - \beta_l(\omega))\frac{L}{\epsilon^2}} e^{i\beta_l(\omega) z^s - i\beta_j(\omega) z_0} \phi_l(x^s) \phi_j(x_0) \times$$
$$e^{(-D_j(\omega) + iO_j(\omega))L} d\omega, \qquad (3.5)$$

where

$$D_j = \frac{\omega^4}{8c_0^4} \sum_{l=1}^{N(\omega)} \frac{1}{\beta_j \beta_l} \int_{-\infty}^{\infty} \cos\left((\beta_j - \beta_l)z\right) \mathbb{E}[C_{jl}(0) C_{jl}(z)] dz,$$

and

$$O_j = -\frac{\omega^4}{8c_0^4} \sum_{l \neq j}^{N(\omega)} \frac{2}{\beta_j \beta_l} \int_{0}^{\infty} \sin\left((\beta_j - \beta_l)z\right) \mathbb{E}[C_{jl}(0) C_{jl}(z)] dz$$
$$+ \frac{\omega^4}{4c_0^4} \sum_{l' > N} \frac{1}{\beta_l' \beta_j} \int_{-\infty}^{\infty} \cos\left(\beta_j s\right) e^{-\beta_{l'}|s|} \mathbb{E}[C_{jl'}(0) C_{jl'}(s)] ds,$$

and where we used (2.57) for $\hat{a}_{j,0}$.

The exponential decay of the mean mode amplitudes means that we loose coherence. Naturally, since we use a coherent imaging method, we look at the case where some coherence is left, that is, $\mathbb{E}[\mathcal{I}^{MIG}] \neq 0$.

It is also important to study the variance of the imaging function

$$\mathbb{E}\left[\left|\mathcal{I}^{(MIG)}(x^s, z^s) - \mathbb{E}[\mathcal{I}^{(MIG)}(x^s, z^s)]\right|^2\right],$$

as it gives a measure of how the imaging depends on the random fluctuations. The imaging function is stable or self-averaging if its variance is zero. This may be the case in limit $\epsilon \to 0$.

3.4 Numerical Results

3.4.1 Code description

The Montjoie software package is used to solve the acoustic wave equation in time domain. This package is developed in INRIA Rocquencourt and our work is done in collaboration with Marc Duruflé. A full documentation of the software can be found in the Montjoie user guide [1].

The temporal source $g(t)$ is a Ricker (second derivative of a Gaussian) with central frequency $f_0 = 1$ KHz , given by

$$g(t) = [2\pi^2(f_0 t - 1)^2 - 1] e^{-\pi^2 (f_0 t - 1)^2}.$$

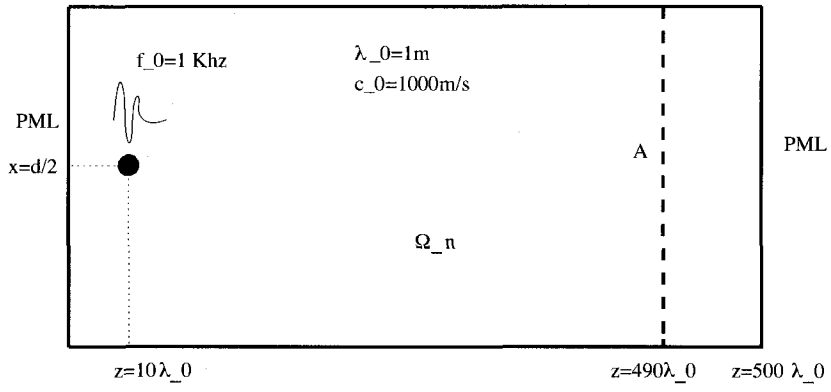

Figure 3.2: Setup for the numerical experiments

The background speed is taken to be a constant $c_0 = 1$ Km/s, so the central wavelength is $\lambda_0 = 1$ m. To simulate a point source in space, a Gaussian distribution with radius $R = 2\lambda_0$ is taken.

The computational domain is a rectangle of length $500\lambda_0$ and width $20\lambda_0$ (See figure 3.2). To simulate an unbounded domain, a perfectly matched layer (PML) is used on the right and left sections of the waveguide, i.e. at $x = 0$ and $x = 500\lambda_0$ respectivley [12, 7]

The code uses Finite Elements with a regular mesh consisting of quadrilaterals. One element per typical wavelength λ_0 is used. The numerical solution, restricted to each quadrilateral, lies in the space Q_8 of polynomials of degree less or equal to 8. The numerical solution is expressed as linear combination of basis functions, that are Lagrange polynomials, with Gauss-Lobatto interpolation points. Mass-lumping is used.

The time scheme is a Leap-Frog scheme of fourth order. Convergence tests for the time scheme can be found in [11].

The fluctuations are modeled using a random Fourier series with a Gaussian correlation function

$$R(x, x', z) = \frac{1}{2\pi l^2} \exp\Big(- \frac{z^2 + (x - x')^2}{2l^2} \Big),$$

correlation length $l = \frac{\lambda_0}{2}$ and $\epsilon = 0.03$.

We conduct three different experiments with different depths $d = 20, 40, 60\lambda_0$. In each experiment, the source is placed at $(z_0 = 10\lambda_0, x_0 = \frac{d}{2}\lambda_0)$. The antenna is placed at a range distance $Z = 490\lambda_0$, where $10 \times d$ receivers are spaced $\frac{\lambda_0}{10}$ apart. The pressure field is measured in the time interval $[0, 2000\,\text{ms}]$. We choose this interval as to include many modes (see Figure 3.7). The search domain of the images is $\Omega_s = [0, d] \times [7, 13\lambda_0]$.

3.4.2 The Effect of Reducing Aperture on Imaging in a Homogeneous Waveguide

In the case where the array is centered at $\frac{d}{2}$ and extends from $\frac{d}{2} - \frac{a}{2}$ to $\frac{d}{2} + \frac{a}{2}$, the coefficients M_{lj} in (3.6) are given by

$$\begin{aligned} M_{lj} =& \frac{1}{d}\Big\{\frac{\sin[(\lambda_l - \lambda_j)(\frac{d+a}{2})] - \sin[(\lambda_l - \lambda_j)(\frac{d-a}{2})]}{(\lambda_l - \lambda_j)} \\ &+ \frac{\sin[(\lambda_l + \lambda_j)(\frac{d-a}{2})] - \sin[(\lambda_l + \lambda_j)(\frac{d+a}{2})]}{(\lambda_l + \lambda_j)}\Big\} \quad \text{for } l \neq j, \\ M_{jj} =& \frac{1}{d}\Big\{a + \frac{\sin[(\lambda_j)(d-a)] - \sin[(\lambda_j)(d+a)]}{(2\lambda_j)}\Big\} \end{aligned} \tag{3.6}$$

In Figure 3.3, we show the matrix M for different array sizes. When the array occupies the whole depth of the waveguide, this matrix is the identity matrix. As the aperture decreases, the entries become spread out but are still concentrated near the diagonal (with higher values for the lower modes). Figure 3.4 shows the effect of aperture on the crossrange focusing of the images (at fixed frequency) in a homogeneous waveguide. As the aperture is reduced, the sidelobes become more significant and the crossrange resolution worsens. The numerical results corroborate the theoretical plots, see Figure 3.5.

3.4.3 The Effect of the Clutter

We compare the pressure fields in a homogeneous and random waveguides of depth $d = 20\lambda_0$. Figure 3.6 shows the pressure at fixed time $t = 1600$ ms. We can still see a coherent wavefront in the random waveguide but it is significantly polluted by the clutter. Figure 3.7 illustrates the effect of the clutter on the time traces of the pressure at the antenna receiver situated at $x = d/2$. Observe the damping of the modes in the clutter and note how the higher modes are damped more than the lower ones.

Figures 3.8 and 3.9 show the damping coefficient D_j and phase shift coefficient, O_j, as a function of mode number for two different frequencies, $f = 0.5$ KHz and $f = 1$ KHz. Note that the damping increases with mode number, since there is more loss of energy due to multiple reflections. We also note that this damping is more significant for higher frequencies.

Figures 3.10 and 3.11 show images at two different fixed frequencies ($f = 0.5$ KHz and $f = 1$ KHz). For the higher frequency, we display the images for three realizations of μ and compare those to the homogenous waveguide. We see that in clutter, there is virtually no focusing for any of the three realizations, whereas the focusing is evidently better in the homogeneous waveguide. For the lower frequency, we see better focusing for the three realizations. This illustrates the stronger damping for higher frequencies. However, the images still do not look stable.

Figures 3.12 and 3.13 show the effect of larger depths on the image. These appear to be more stable compared to Figures 3.10 and 3.11. For the same fixed frequency, larger depths amount to larger number of modes (as seen in (2.18)).

Figure 3.14 shows the effect of broadband. Summing over a frequency band with 50 frequencies between $0.5 - 0.5245$, gives more stable images (compared to the fixed frequency case). We choose this band as to be consistent with the broadband scaling in [13], and to guarantee that we have a fixed number of modes. We compare the

expectation of the image to the image obtained in the homogeneous waveguide. The spot size in the range direction is slightly larger than the spot size in the homogeneous waveguide. This is explained by the fact that the clutter introduces a shift in the arrival time of the modes, encoded in the O_j coefficients. Integrating over frequency averages these shifts and yields a broader spot.

3.5 Research Plan

We want to study theoretically the stability and focusing properties of the imaging function $\mathcal{I}^{(MIG)}$. This will be done in both broadband and narrowband regimes.

- In the broadband case, the stability should follow easily because the mode amplitudes decorrelate for frequencies that are more than ϵ^2 apart, as shown in [13].
- In the narrowband case, if stability holds, it will be due to the averaging over many modes as suggested by Figures 3.12 and 3.13. For that, we need the second moments of the modes amplitudes, given by Proposition 3.
- In the case where stability holds, we wish to quantify the loss of resolution and see if we can improve the imaging at least for a point source.

We wish to study coherent interferometric methods [4, 5, 6] for imaging sources in waveguides. These methods work with cross-correlations of the signals at the array, which are supposed to emphasize the coherent part of the signal and diminish the clutter. We also want to image sources emitting stationary random signals. In this case, the data at the array has no coherent part at all, so we want to do the imaging using cross-correlations [14].

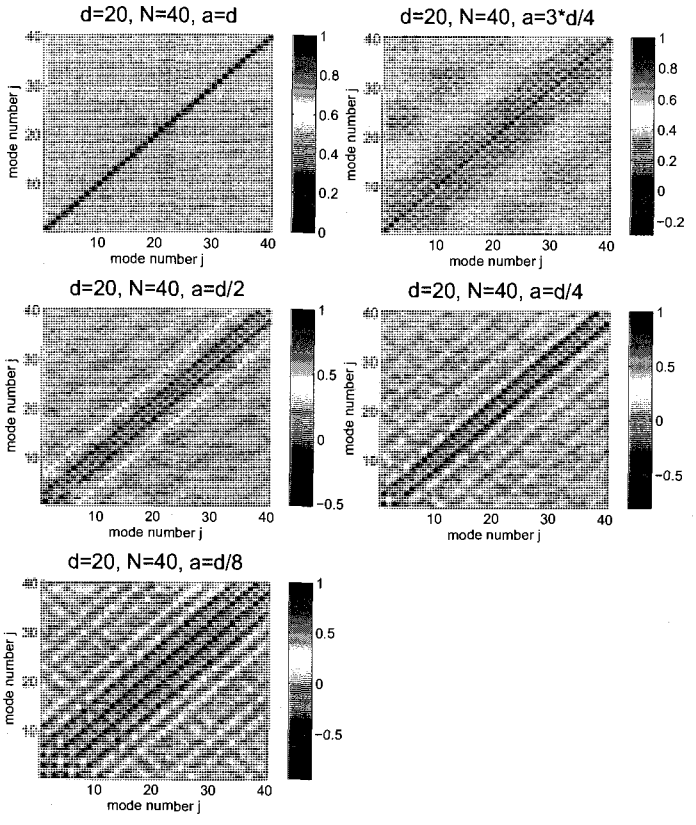

Figure 3.3: Array matrix M_{lj}. $N = 40$ modes, depth $d = 20\lambda_0$ and array sizes $a = d, \frac{3d}{4}, \frac{d}{2}, \frac{d}{4}$ and $\frac{d}{8}$.

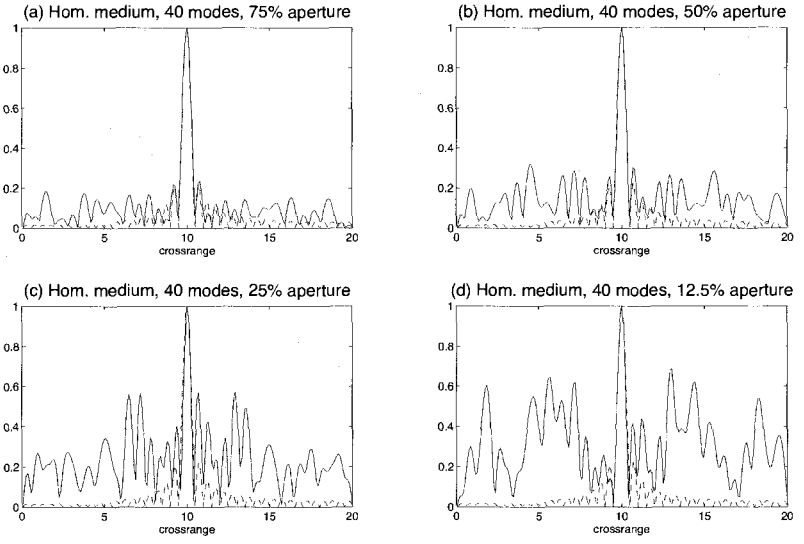

Figure 3.4: Normalized cross range profiles (by max norm) from theory. Cross range in λ_0. Dotted blue line corresponds to $a = d$, solid red lines correspond to (a) $a = \frac{3d}{4}$, (b) $a = \frac{d}{2}$, (c) $a = \frac{d}{4}$ and (d) $a = \frac{d}{8}$.

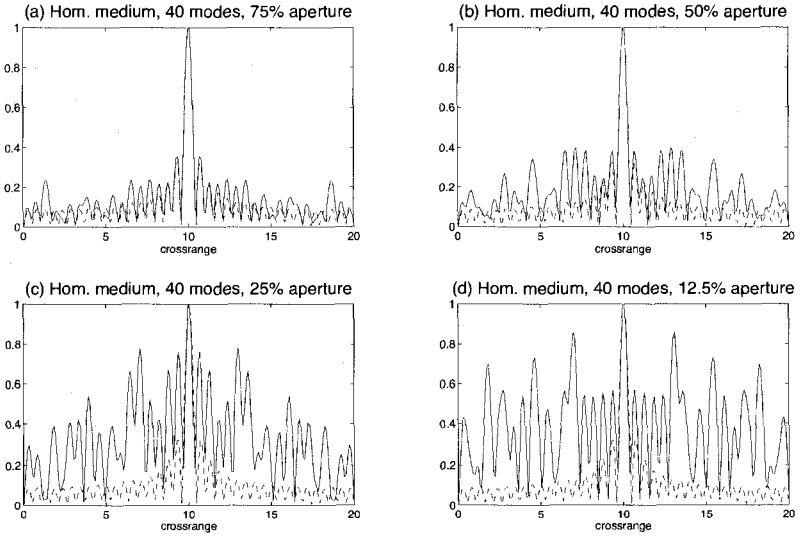

Figure 3.5: Normalized cross range profiles (by max norm) from code. Cross range in λ_0. Dotted blue line corresponds to $a = d$, solid red lines correspond to (a) $a = \frac{3d}{4}$, (b) $a = \frac{d}{2}$, (c) $a = \frac{d}{4}$ and (d) $a = \frac{d}{8}$.

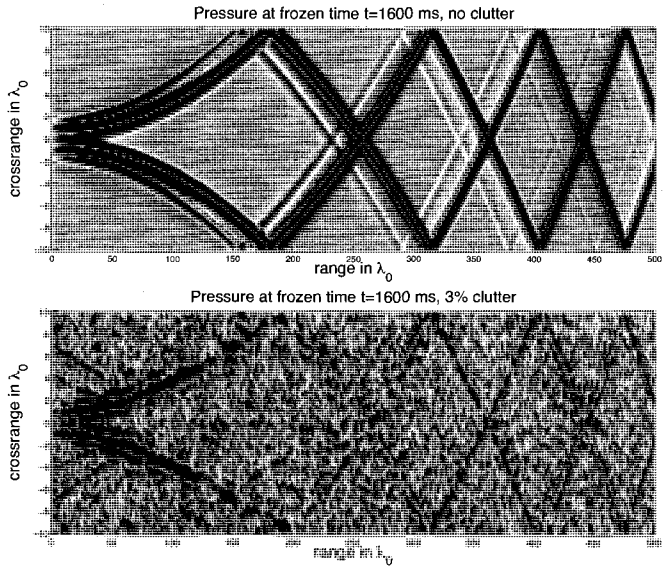

Figure 3.6: 2D snapshots in homogeneous (top) and cluttered (bottom) waveguide with $\epsilon = 0.03$.

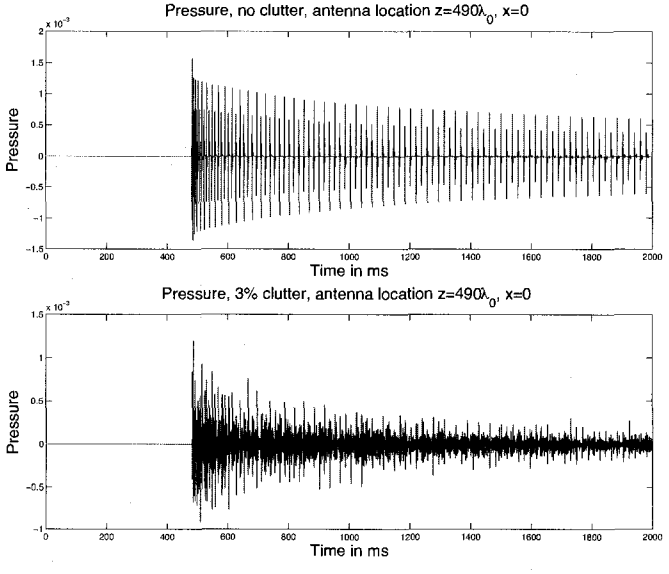

Figure 3.7: Time traces for homogeneous (top) and cluttered (bottom) waveguide with $\epsilon = 0.03$.

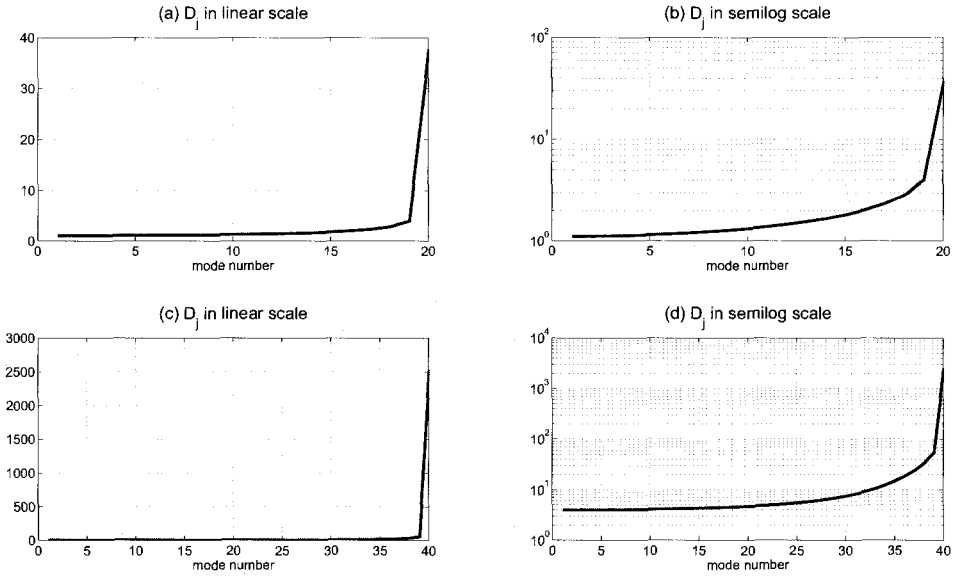

Figure 3.8: Damping coefficient D_j. In linear (left) and semi-log scale (right) for $f = 0.5$ KHz (top) and $f = 1$ KHz (bottom)

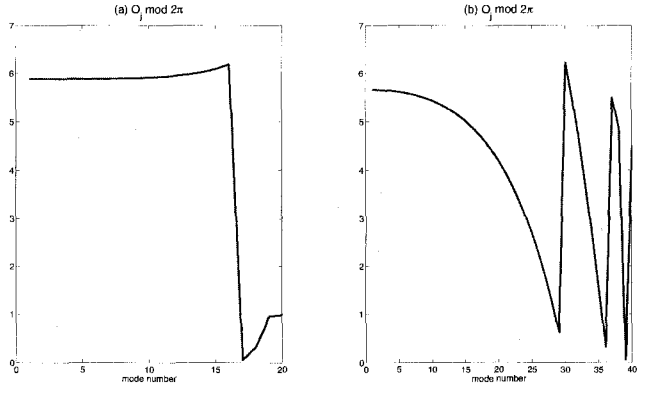

Figure 3.9: Phase shift coefficient O_j (mod 2π). (a) $f = 0.5$ KHz and (b) $f = 1$ KHz

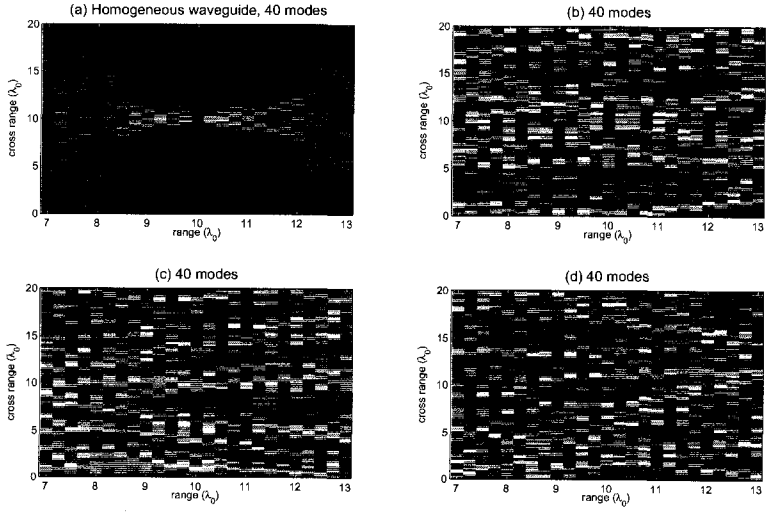

Figure 3.10: Images at fixed frequency $f = 1\,\text{KHz}, d = 20\lambda_0$ and $N = 40$. (a) shows the case for a homogeneous waveguide. Three realizations of μ, with $\epsilon = 0.03$ are shown in (b), (c), (d).

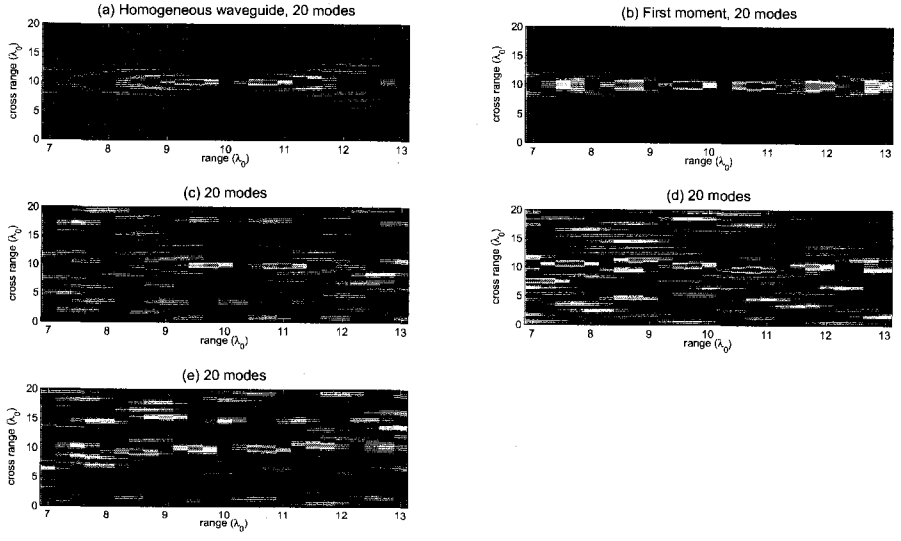

Figure 3.11: Images at $f = 0.5\,\text{KHz}, d = 20\lambda_0$ and $N = 20$. (a) Shows the case for a homogeneous waveguide. Three realizations of μ, with $\epsilon = 0.03$. are shown in (c),(d), and (e). The expectation of the image is shown in (b).

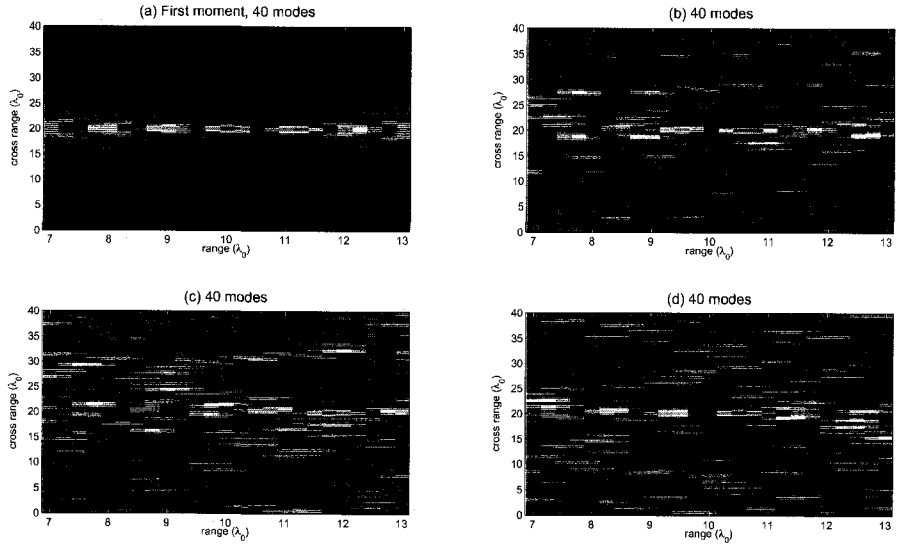

Figure 3.12: Images in a cluttered waveguide with $d = 40\lambda_0$, $f = 0.5$ KHz and $N = 40$. First moment (top left) and three realizations of μ, with $\epsilon = 0.03$.

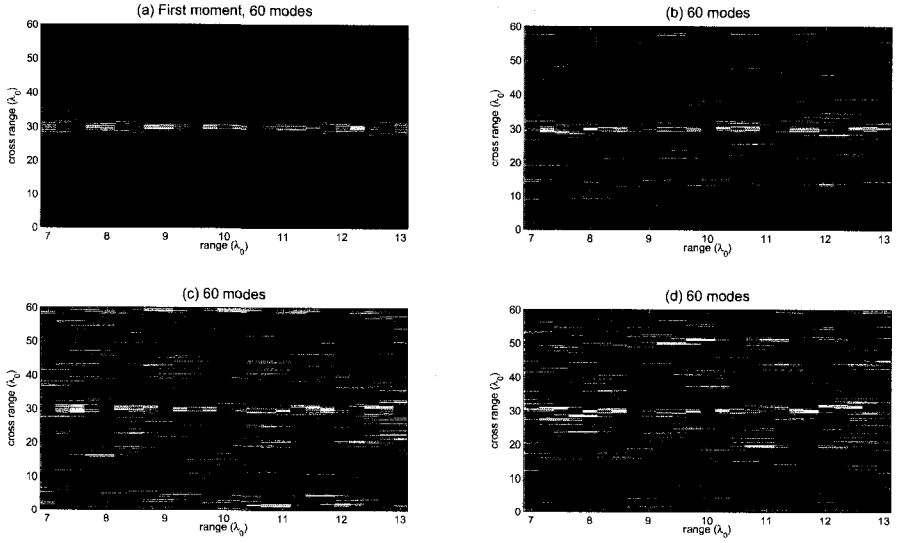

Figure 3.13: Images in a cluttered waveguide with $d = 60\lambda_0$, $f = 0.5$ KHz and $N = 60$. First moment (top left) and three realizations of μ, with $\epsilon = 0.03$.

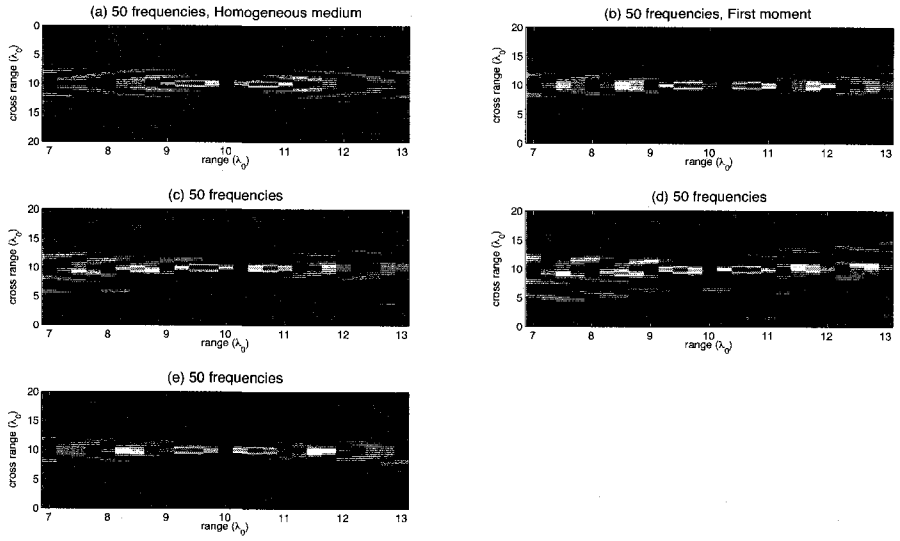

Figure 3.14: Broadband images in a cluttered waveguide (50 frequencies between $0.5 - 0.5245$ KHz), $d = 20\lambda_0$ and $N = 20$. The homogeneous medium is shown in (a) for comparison. The first moment is shown in (b). Three realizations of μ with $\epsilon = 0.03$ are shown in (c), (d), and (e).

Appendix A

The Diffusion Limit

A.1 Statement of the Theorem

Theorem 1. *(Kashminski) Let the process $X(z) \in \mathbb{R}^d$ be defined by the system of random ordinary differential equations*

$$\begin{aligned} \frac{dX}{dz}(z) &= \epsilon \mathcal{F}(X, z, w, \epsilon), \\ X(0) &= x_0, \end{aligned} \tag{A.1}$$

where $\mathcal{F}(X, z, w, \epsilon) \in \mathbb{R}^d$, $z \geq 0$. Let $(\Omega_p, \mathcal{M}, \mathbb{p})$ be a probability space with $w \in \Omega_p$. Suppose that $\mathcal{F}$ satisfies

$$\mathcal{F}(X, z, w) = \mathcal{H}(X, z, w) + \epsilon \mathcal{G}(X, z, w) + O(\epsilon^2),$$

*where $\mathcal{H}$ and $\mathcal{G}$ are measurable stochastic processes that are bounded, along with their first and second derivatives w.r.t to x. Assume that $\mathcal{F}$ is **mixing** and that the following limits exist and are uniform in x and z^**

$$\lim_{Z \to \infty} \frac{1}{Z} \int_{z^*}^{z^*+Z} \mathbb{E}[\mathcal{H}(x, t, w)] dt = 0,$$

$$\lim_{Z \to \infty} \frac{1}{Z} \int_{z^*}^{z^*+Z} \mathbb{E}[\mathcal{G}(x, t, w)] dt = \bar{\phi}^{(1)}(x),$$

$$\lim_{Z\to\infty}\frac{1}{Z}\int_{z^*}^{z^*+Z}\int_{z^*-Z}^{s}\mathbb{E}[(\mathcal{H}(x,t,w)\cdot\nabla_x)\,\mathcal{H}(x,s,w)]dtds=\bar{K}(x)$$

and

$$\lim_{Z\to\infty}\frac{1}{Z}\int_{z^*}^{z^*+Z}\int_{z^*}^{z^*+Z}\mathbb{E}[\mathcal{H}_j(x,s,w)\mathcal{H}_k(x,t)]dtds=\bar{a}_{j,k}(x),$$

Then the scaled process $X^\epsilon=X(\frac{z}{\epsilon^2})$ *given by the system*

$$\frac{dX^{(\epsilon)}}{dz}(z)=\frac{1}{\epsilon}\mathcal{H}(X^{(\epsilon)}(z),\frac{z}{\epsilon^2},w)+\mathcal{G}(X^{(\epsilon)}(z),\frac{z}{\epsilon^2},w),\tag{A.2}$$

converges weakly in the interval $0\le z\le L$ *to a Markov process* X^0*, which is continuous with probability one, and which can be described as the solution of*

$$dX^0(z)=b(X^0(z))dz+\sigma(X^0(z))dW(z),$$

where

$$b(x)=\bar{K}(x)+\bar{\phi}^{(1)}(x),$$

$$(\sigma(x)\sigma^*(x))_{jk}=\bar{a}_{j,k}(x),$$

and $W(z)=\big(w_1(z),...w_d(z)\big)$ *are independent standard Brownian motion.*

A.2 Application of the Diffusion Limit to the Stochastic Mode Equations

We consider jointly the vector $\hat{\mathbf{a}}$ and its complex conjugate $\overline{\hat{\mathbf{a}}}$, which satisfies the complex conjugate of equation (2.56). We do that because it is more convenient to work with the mode amplitudes and their conjugates, rather than with their real and imaginary parts. Define the vector

$$X^\epsilon=\begin{pmatrix}\hat{\mathbf{a}}^\epsilon\\ \overline{\hat{\mathbf{a}}^\epsilon}\end{pmatrix}\quad\in\mathbb{C}^{2N},$$

and for the complex variable $\zeta=x+iy$, define the complex derivatives as

$$\partial_\zeta=\frac{1}{2}(\partial_x-i\partial_y),\quad \partial_{\overline{\zeta}}=\frac{1}{2}(\partial_x+i\partial_y).$$

Now write (2.50) in the form

$$\frac{dX^\epsilon}{dz} = \frac{1}{\epsilon}\mathcal{H}(X^\epsilon, \frac{z}{\epsilon^2}) + \mathcal{G}(X^\epsilon, \frac{z}{\epsilon^2}). \tag{A.3}$$

Here

$$\mathcal{H}(X,z) = \begin{pmatrix} \mathbf{H}^{aa}(z)\hat{\mathbf{a}} \\ \overline{\mathbf{H}^{aa}}(z)\bar{\hat{\mathbf{a}}} \end{pmatrix}, \quad \mathcal{G}(X,z) = \begin{pmatrix} \mathbf{G}^{aa}(z)\hat{\mathbf{a}} \\ \overline{\mathbf{G}_{aa}}(z)\bar{\hat{\mathbf{a}}} \end{pmatrix}$$

where the entries of $\mathbf{H}^{(aa)}(z)$ and $\mathbf{G}^{(aa)}(z)$ are given by

$$H_{jl}^{(aa)}(z) = \frac{ik^2}{2}\frac{C_{jl}(z)}{\sqrt{\beta_j\beta_l}}e^{i(\beta_l-\beta_j)z},$$

and

$$G_{jl}^{(aa)}(z) = \frac{ik^4}{4}\sum_{l'>N}\int_{-\infty}^{\infty}\frac{C_{jl'}(z)C_{ll'}(z+s)}{\sqrt{\beta_j\beta_{l'}^2\beta_l}}e^{i\beta_l(z+s)-i\beta_j(z)-\beta_{l'}|s|}ds,$$

with

$$C_{jl}(z) = \int_0^d \phi_j(x)\phi_l(x)\mu(z,x)dx.$$

The mixing assumption requires that $\mu(x,z)$ and $\mu(x',z+s)$ are statistically independent for large s: this is why we need the assumption that the correlation function of μ decays in range.

A.3 Derivation of the Generator

From Theorem 1, the generator of the limiting Markov process is given by

$$\begin{aligned}\mathcal{L} &= (K(\bar{X}) + \bar{\phi}^{(1)}(X))\cdot\nabla_X \\ &= \lim_{Z\to\infty}\{\frac{1}{Z}\int_{z^*}^{z^*+Z}\int_{z^*}^{s}\mathbb{E}\left[(\mathcal{H}(X,t)\cdot\nabla_X)\mathcal{H}(X,s)\right]\cdot\nabla_X dtds \\ &+ \frac{1}{Z}\int_{z^*}^{z^*+Z}\mathbb{E}\left[\mathcal{G}(X,t)\cdot\nabla_X\right]dt + \int_{z^*}^{z^*+Z}\int_{z^*}^{s}\sum_{j,k}\mathbb{E}\left[\mathcal{H}(X,t)\mathcal{H}(X,s)^\top\right]\frac{\partial^2}{\partial X_j\partial X_k}dtds\}.\end{aligned} \tag{A.4}$$

To make the notation easier, we let $\tilde{C}_{jl} = \frac{k^2}{2}\frac{C_{jl}(z)}{\sqrt{\beta_j\beta_l}}e^{i(\beta_l-\beta_j)z}$. Recalling the expressions for $\mathcal{H}$ and $\mathcal{G}$, we obtain

$$\mathcal{L} = \mathcal{L}_1 + \mathcal{L}_2 + \mathcal{L}_3 + c.c.$$

where c.c stands for complex conjugate and where

$$\mathcal{L}_1 = -\sum j,l \sum j',l' \{ \lim_{Z\to\infty} \frac{1}{Z} \int_{z^*}^{z^*+Z} ds \int_{z^*}^{s} dt\, E[\tilde{C}_{jl}(t)\tilde{C}_{j'l'}(s)] \times e^{i(\beta_l-\beta_l)t+i(\beta_{l'}-\beta_{j'})s} \hat{a}_l \frac{\partial}{\partial \hat{a}_j} (\hat{a}_{l'} \frac{\partial}{\partial \hat{a}_{j'}}) \}, \tag{A.5}$$

$$\mathcal{L}_2 = \sum_{j,l} \sum_{j',l'} \{ \lim_{Z\to\infty} \frac{1}{Z} \int_{z^*}^{z^*+Z} ds \int_{z^*}^{s} dt\, E[\tilde{C}_{jl}(t)\tilde{C}_{j'l'}(s)] e^{i(\beta_l-\beta_j)t-i(\beta_{l'}-\beta_{j'})s} \hat{a}_l \frac{\partial}{\partial \hat{a}_j} (\hat{a}^*_{l'} \frac{\partial}{\partial \hat{a}^*_{j'}}) \}$$

and

$$\mathcal{L}_3 = -\sum_{j,l} \{ \lim_{Z\to\infty} \frac{1}{Z} \int_{z^*}^{z^*+Z} ds \sum_{l'>N} \int_{-\infty}^{\infty} dt\, E[\tilde{C}_{jl}(t+s)\tilde{C}_{j'l'}(t)] e^{i(\beta_l(s+t)-\beta_j t)} e^{-\beta_{l'}|t|} \hat{a}_l \frac{\partial}{\partial \hat{a}_j} \}$$

Making the change of variables $\tau = s - t$, $s = s$, and taking the limit as $Z \to \infty$, we get

$$\mathcal{L}_1 = -\sum_{j,l} \sum_{j',l'} \left[\int_0^{\infty} d\tau E[\tilde{C}_{jl}(\tau)\tilde{C}_{j'l'}(0)] e^{i(\beta_j-\beta_l)\tau \hat{a}_l \frac{\partial}{\partial \hat{a}_j}} (\hat{a}_{l'} \frac{\partial}{\partial \hat{a}_j}) \right] \times \left[\lim_{Z\to\infty} \frac{1}{Z} \int_{z^*}^{z^*+Z} ds\, e^{is[(\beta_l-\beta_l)+(\beta_{l'}-\beta_{j'})]} \right]. \tag{A.6}$$

The limit of the last integral is zero unless $\beta_l - \beta_j + \beta_{l'} - \beta_{j'} = 0$.

So we have,

$$\mathcal{L}_1 = -\sum_{\beta_l-\beta_j=\beta_{j'}-\beta_{l'}} \{ \int_0^{\infty} d\tau E\{\tilde{C}_{jl}(\tau)\tilde{C}_{j'l'}(0)\} e^{(\beta_j-\beta_l)\tau} \} \hat{a}_l \frac{\partial}{\partial \hat{a}_j} (\hat{a}_{l'} \frac{\partial}{\partial \hat{a}_j}).$$

Similarly, for $\mathcal{L}_2$, and $\mathcal{L}_3$, we get

$$\mathcal{L}_2 = \sum_{\beta_l-\beta_j=\beta_{l'}-\beta_{j'}} \{ \int_0^{\infty} d\tau E[\tilde{C}_{jl}(\tau)\tilde{C}_{j'l'}(0)] e^{(\beta_j-\beta_l)\tau} \} \hat{a}_l \hat{a}^*_{l'} \frac{\partial^2}{\partial \hat{a}_j \partial \hat{a}^*_{j'}},$$

and

$$\mathcal{L}_3 = \sum_{l'>N} \{ \int_{-\infty}^{\infty} d\tau\, E[\tilde{C}_{jl'}(0)\tilde{C}_{j'l'}(\tau)] e^{i\beta_j\tau} e^{-\beta_{l'}|\tau|} \} \hat{a}_j \frac{\partial}{\partial \hat{a}_j}$$

Combining these expressions with their complex conjugates, we get the desired result for the generator.

Bibliography

[1] *MONTJOIE's user guide.*

[2] A Baggeroer, W Kuperman, and P Mikhalevsky. An overview of matched field methods in ocean acoustics. *IEEE Journal of Oceanic Engineering*, 18:401–424, 1993.

[3] A.B. Baggeroer, W.A Kuperman, and Henrik Schmidt. Matched field processing: Source locatization in correlated noise as an optimum parameter estimation problem. *J.of the Acoustical Soc. of Amer.*, 83(2), 1988.

[4] Liliana Borcea, George Papanicolaou, and Tsogka Chrysoula. Coherent interferometric imaging. *Geophysics*, 71:S1165–S1175, 2006.

[5] Liliana Borcea, George Papanicolaou, and Chrysoula Tsogka. Interferometric array imaging in clutter. *Inverse Problems*, 21:1419–1460, 2005.

[6] Liliana Borcea, George Papanicolaou, and Chrysoula Tsogka. Adaptive interferometric imaging in clutter and optimal illumination. *Inverse problems*, 22:1405–1436, 2006.

[7] G Cohen. *Higher-order numerical methods for transient wave equations.* Springer Verlag, 2002.

[8] S Dediu. *Recovering inhomogeneities in a waveguide using eigensystem decomposition.* PhD thesis, Rensselaer Polytechnic Institute, 2005.

[9] Sava Dediu and Joyce McLaughlin. Recovering inhomogeneities in a waveguide using eigensystem decomposition. *Inverse Problems*, 22:pp.1227–1246, 2006.

[10] L.B Dozier and F Tappert. Statistics of normal mode amplitudes in a random ocean. *J.Acoust.Soc.Am*, 63(2), Feb. 1978.

[11] Marc Duruflé. Application de la technique dite de l'équation modifiée à l'équation des ondes avec des conditions absorbantes et des couches pml. Technical report, I.N.R.I.A Rocquencourt, 2004.

[12] Marc Duruflé. *Intégration numérique et éléments finis d'ordre élevé appliqués aux équations de Maxwell en régime harmonique.* PhD thesis, Université Paris Dauphine, 2006.

[13] J-P Fouque, J Garnier, Papanicolaou G., and K Solna. *Wave Propagation and Time Reversal in Randomly Layered Media.* Springer, 2007.

[14] Josselin Garnier. Imaging in randomly layered media by cross-correlating noisy signals. *SIAM Multiscale model.simul*, 4:610–640, 2005.

[15] Josselin Garnier and George Papanicolaou. Pulse propagation and time reversal in random waveguides. *AMS subject classifications*, 2006.

[16] R Gilbert and Y. Lin. Scattering in a shallow ocean with a an elastic sea-bed. *Comput. Acoust.*, 5:403–431, 1997.

[17] R Gilbert, M Werby, and Y. Xu. Determination of a buried object in a two-layered shallow ocean. *Journal of computational acousitcs*, 9:1025–1037, 2001.

[18] R Gilbert and Y. Xu. Acoustic imaging in a shallow ocean with a thin cap. *Inverse problems*, 16:1799–1811, 2000.

[19] R.Z Kashminski. A limit theorem for the solutions of differential equations with random right hand sides. *Theory of probability and applications*, 1966.

[20] E Kirr and M.I Weinstein. Diffusion of power in randomly perturbed hamiltonian partial differential equations. 2004.

[21] Werner Kohler and George Papanicolaou. Wave propagation is a randomly inhomogeneous ocean. *Lecture Notes in Physics*, 70:153–223, 1977.

[22] William Kuperman and Darrel Jackson. *Ocean Acoustics, Matched-Field Processing and Phase Conjugation.* Springer-Verlag Berlin Heidelberg, 2002.

[23] W.H. Munk. Sound channel in an exponentially stratifed ocean, with applications to sofar. *J.Acoust. Soc. Am*, 55:220–226, 1974.

[24] J Papadakis, M Taroudakis, and P Papadakis. A new method for a realistic treatment of the sea bottom in the parabolic approximation. *Journal of the Acoustic Society of America*, 1992.

[25] G. Papanicolaou. Asymptotic analysis of stochastic equations. *Studies in Probability Theory*, 18:111–179, 1978.

[26] M.B Priestley. *Spectral And Mathematical Statistics.* Academic Press, 1981.

[27] W. Symes. A differential semblance criterion for inversion of multioffset seismic reflection data. *J. Geophys. Res.*, 88, 1993.

[28] F.D Tappert. The parabolic approximation method. *Lectures Notes in Physics*, 70:Chapter V.